

Enhancing disaster risk resilience using greenspace in urbanising

Quito, Ecuador

C. Scott Watson¹, John R. Elliott¹, Susanna K. Ebmeier¹, María Antonieta Vásquez², Camilo Zapata², Santiago Bonilla-Bedoya³, Paulina Cubillo⁴, Diego Francisco Orbe⁴, Marco Córdova⁵, Jonathan Menoscal⁵, Elisa Sevilla²

¹COMET, School of Earth and Environment, University of Leeds, Leeds, LS2 9JT, UK.

²College of Social Sciences and Humanities, Universidad San Francisco de Quito, Quito 170901, Ecuador.

³Research Center for the Territory and Sustainable Habitat, Universidad Tecnológica Indoamérica, Machala y Sabanilla, 170301, Quito, Ecuador.

⁴Centro de Información Urbana de Quito - CIUQ, Quito, Ecuador.

⁵Facultad Latinoamericana de Ciencias Sociales - Flacso, Quito, Ecuador.

Correspondence to: C. Scott Watson (c.s.watson@leeds.ac.uk)

Abstract

Greenspaces within broader ecosystem-based disaster risk reduction strategies (Eco-DRR) provide multiple benefits to society, biodiversity, and addressing climate breakdown. In this study, we investigated urban growth, its intersection with hazards, and the availability of greenspace for disaster risk reduction (DRR) in the city of Quito, Ecuador, which experiences multiple hazards including landslides, floods, volcanoes, and earthquakes. We used satellite data to quantify urban sprawl and developed a workflow incorporating high resolution digital elevation models (DEMs) to identify potential greenspaces for emergency refuge accommodation (DRR greenspace), for example following an earthquake. Quito's historical urban growth totalled ~192 km² 1986–2020 and was primarily on flatter land, ~~in some cases, crossed by~~ steep ravines. By contrast, future projections indicate an increasing intersection between easterly urbanisation and steep areas of high landslide susceptibility. Therefore, a timely opportunity exists for future risk-informed planning. Our workflow identified 18.6 km² of DRR greenspaces, of which 16.3 km² intersected with potential sources of landslide and flood hazards, indicating that hazard events could impact potential 'safe spaces'. These spaces could mitigate future risk if designated as greenspaces and left undeveloped. DRR greenspace overlapped 7% (2.5 km²) with municipality designated greenspace. Similarly, 10% (1.7 km²) of municipality designated 'safe space' for use following an earthquake was classified as potentially DRR suitable in our analysis. For emergency refuge, currently designated greenspaces could accommodate ~2–14% ~~(depending on space requirements)~~ of Quito's population within 800 m. This increases to 8–40% considering all the potential DRR greenspace

Deleted:

Deleted: deep

33 mapped in this study. Therefore, a gap exists between the provision of DRR and designated greenspace. Within Quito, we
34 found a disparity between access to greenspaces across socio-economic groups with lower income groups having less access
35 and further to travel to designated greenspaces. Notably, the accessibility of greenspaces was high overall with 98% (2.3
36 million) of Quito's population within 800 m of a designated greenspace, of which 88% (2.1 million) had access to potential
37 DRR greenspaces. Our workflow demonstrates a citywide evaluation of DRR greenspace potential and provides the
38 foundation upon which to evaluate these spaces with local stakeholders. Promoting equitable access to greenspaces,
39 communicating their multiple benefits, and considering their use to restrict propagating development into hazardous areas
40 are key themes that emerge for further investigation.

41 **1 Introduction**

42 Urbanising and increasing populations are a global trend that create a range of societal and environmental challenges
43 including food and water security (Godfray et al., 2010; Hoekstra et al., 2018), air pollution (Fenger, 1999; Escobedo and
44 Nowak, 2009; Zalakeviciute et al., 2018), disease (Marmot et al., 2008), loss of biodiversity (McDonald et al., 2020), climate
45 change (De Sherbinin et al., 2007; Flörke et al., 2018), and exposure to disaster risk (Pelling et al., 2004). Approximately
46 68% of the world's population are projected to live in urban areas by 2050, many of which are yet to be developed, and the
47 rate of urbanisation is greatest for developing countries (UN DESA, 2019). Development of informal settlements takes place
48 outside of regulatory frameworks such as land use planning or building design codes (UN-Habitat, 2003; Oliver-Smith et al.,
49 2016). Therefore, urbanisation often occurs within or creates hazardous areas, which exacerbates the socioeconomic
50 inequalities of disaster risk due to overcrowding, unsafe housing, and lack of infrastructure and services (Baker, 2012;
51 Cardona et al., 2012). Reducing disaster risk and losses is the aim of the global Sendai Framework for Disaster Risk
52 Reduction 2015–2030 (UNDRR, 2015) and is integral to achieving the UN sustainable development goals (SDGs).
53 Specifically, Goal 11 to 'make cities and human settlements inclusive, safe, resilient and sustainable' targets reducing deaths
54 and socio-economic impacts associated with disasters with a focus on the most vulnerable (UN General Assembly, 2015).
55 Successful risk reduction in 'tomorrow's cities' requires people-centred decision making to support a transition from disaster
56 response to risk-informed planning (Galasso et al., 2021). Additionally, nature-based solutions (NbS) involving greenspace
57 in cities are increasingly recognised within a framework of Ecosystem-based Disaster Risk Reduction (Eco-DRR) (Estrella
58 and Saalimaa, 2013; Faivre et al., 2018; UNDRR, 2020) and can be designed and monitored using an increasing number of
59 earth observation (EO) technologies (Kumar et al., 2021). EO data are widely used for land cover classifications to quantify
60 historical trends in urban expansion and to model future urbanisation projections (Schneider and Woodcock, 2008; Bonilla-
61 Bedoya et al., 2020b). Both high-resolution (< 1 m, commercial) (Myint et al., 2011; Georganos et al., 2018) and medium
62 resolution (10–30 m, open-access) (e.g. Landsat and Sentinel-2) optical satellite imagery are used for land cover and
63 greenspace mapping (Fuller et al., 1994; Labib and Harris, 2018; Deng et al., 2019).

Deleted: (Galasso et al., 2021)

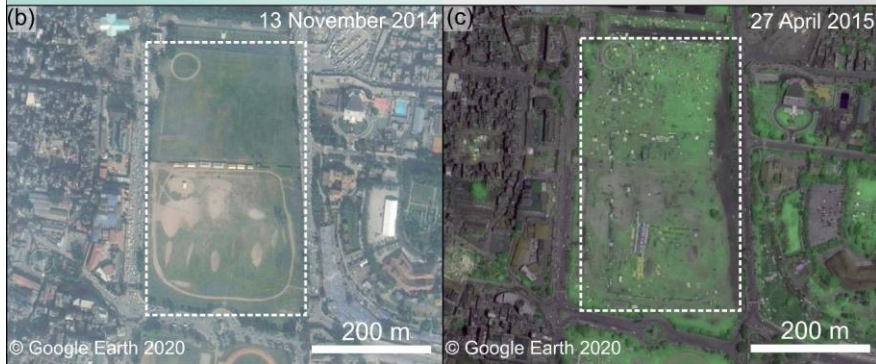
Deleted: the goal of building sustainable cities and communities

67 There are multiple definitions of greenspace, however, they generally include reference to public parks, gardens, open space,
68 wetlands, street verges, woodland, and sports grounds (Taylor and Hochuli, 2017). Greenspace is associated with multiple
69 impacts on urban and natural systems (Fig. 1a) including: improving mental and physical health (James et al., 2015; WHO
70 Regional Office for Europe, 2016; Marselle et al., 2020; Bauwelinck et al., 2021); conserving natural ecosystems and
71 biodiversity (Aronson et al., 2017; McDonald et al., 2020); creating economic opportunities (Gregory McPherson, 1992);
72 building community resilience to hazards (Colding and Barthel, 2013), including reducing landslide risk (Phillips and
73 Marden, 2005; Sandholz et al., 2018) and urban flooding (Maragno et al., 2018); and providing safe spaces in the event of a
74 disaster (Shrestha et al., 2018; Sphere Association, 2018; Shimpo et al., 2019; Jeong et al., 2021). However, greenspace
75 planning in urban environments is often recreation focused (Boulton et al., 2018). Therefore, it is important to recognise the
76 provision of multi-benefit greenspaces within an Eco-DRR framework, and the diverse accessibility, ownership, and
77 management of such spaces (Colding and Barthel, 2013). Similarly, the creation and designation of greenspace requires
78 consideration of social justice issues, such as the impact on property values (Wolch et al., 2014; García-Lamarca et al.,
79 2020).

80
81 Green cities, which incorporate diverse greenspace, green infrastructure, and interconnected social and ecological networks,
82 provide opportunities to enhance disaster resilience and deliver multiple benefits for sustainable development and nature
83 conservation (Benedict and MacMahon, 2002; Tidball and Krasny, 2012). These elements may be designed and integrated
84 into planning policy (Jeong et al., 2021) or emerge following crises, such as loss of food security prompting the proliferation
85 of urban gardening (Altieri et al., 1999; Gonzalez, 2003; Colding and Barthel, 2013). Similarly, following disaster events
86 such as earthquakes, open spaces are used for emergency refuge (Allan et al., 2013; Borland, 2020). The latter point was the
87 case following the 2015 Gorkha earthquake [in Nepal](#), where greenspaces were used for temporary accommodation away
88 from collapsed and damaged buildings (Fig. 1 b-c). Temporary government camps homed over 30,000 people in the
89 Kathmandu Valley and over 1,000 smaller shelter sites homed thousands more (Khazai et al., 2015). Greenspace was also
90 prioritised in Tokyo following the 1923 Great Kantō Earthquake, where parks originally designed to provide space for
91 children were later valued as emergency refuges (Borland, 2020). Innovative greenspace design elements may also emerge
92 following disaster events, such as integrating water bodies and pumps, edible plant species, and multi-purpose (e.g. seating,
93 dining, and cooking) communal seating areas into greenspace areas (Bryant and Allan, 2013).

94
95 Historically, green space in Quito was defined by the rural-urban relationship. Until the end of the 19th century, green spaces
96 were the "Ejidos", sites for agriculture and livestock, which were located on the outskirts of the city. The urbanisation model
97 did not contemplate green spaces in its design and natural spaces such as the ravines were mostly filled in (Aragundi et al.,
98 2016). This is important because parks and plazas have been repeatedly used as refuge sites after earthquakes in Quito. For
99 example, during the 1859 Quito earthquake and 1868 Ibarra earthquake, refugee tents were set in the main plazas and parks

100 of the city (e.g. Figure 1d, e). During the 20th Century, the use of these greenspaces and open spaces like plazas as refuge
101 after earthquakes was recognised through the creation of official 'safe spaces' (see section 4.3) (Metro Ecuador, 2019).



103 **Figure 1: (a) Example impacts of urban greenspace on hazards, health, ecosystems, and infrastructure. (b-c) An area of**
104 **greenspace ‘Tundikhel’ (Lat: 27.702°, Lon: 85.315°) in Kathmandu, Nepal, which was used for temporary tented accommodation**
105 **following the Gorkha earthquake (25 April 2015). (d-e) Tents in Plaza Santo Domingo and Plaza Mayor (Plaza Grande) in Quito**
106 **after the 1868 Ibarra earthquake.**

107
108 Quito has a population of over 2 million (2020), having doubled in just three decades from 1 million in the late 1980s, and
109 which is projected to exceed 3.4 million by 2040 (DMQ, 2018). The expansion of formal and informal settlements into
110 hazardous areas increases disaster risk from events including landslides, flooding, volcanic eruptions, and earthquakes.
111 Increased disaster risk is due to both increased exposure to natural hazards and the social vulnerability of the exposed
112 communities (e.g. Valcárcel et al., 2017). Therefore, in this study we assessed the potential of greenspace for reducing
113 disaster risk in contemporary Quito, and for guiding the development of more resilient communities in future urban areas.
114 Specifically, we: (1) quantified Quito’s recent historical urban expansion using satellite-based optical imagery and evaluated
115 potential future urbanisation scenarios using land classification metrics; (2) investigated the intersection between the built
116 environment and natural hazards; and (3) evaluated the potential role of urban greenspace for reducing disaster risk in Quito
117 by providing ‘safe spaces’. In this study, we analyse a style of greenspace relevant to disaster risk reduction that is
118 quantifiable using optical satellite data. Specifically, we focus on low gradient open spaces that are vegetated. We do not
119 consider specific greenspace amenities such as recreation facilities, or accessibility restrictions, which cannot be determined
120 using satellite data alone.

Deleted: define

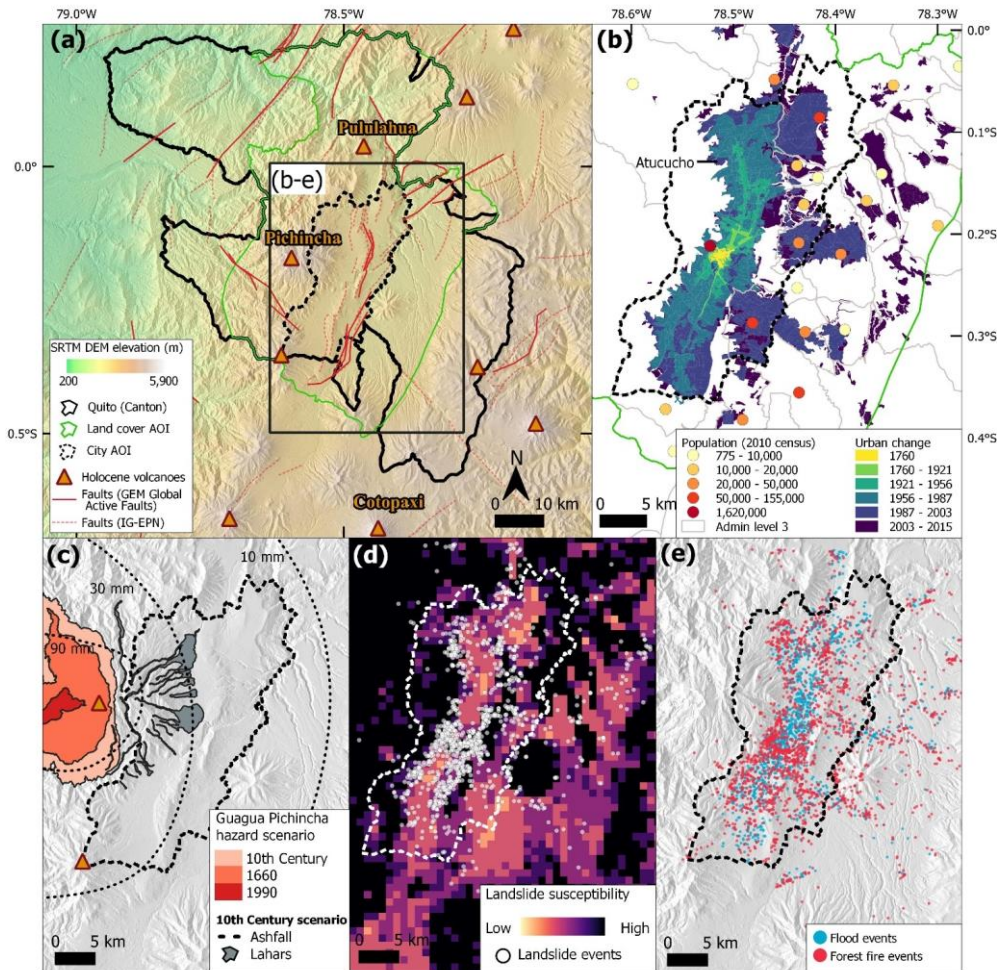
121 2 Study region

122 Quito is situated in the central region of Ecuador, just south of the equator in the Inter-Andean Valley of South America at
123 over 2,800 m a.s.l. and is bounded by Pichincha Volcano (4794 m) to the west and steep topography to the east (Fig. 2).
124 Topography and factors such as the intertropical convergence zone and the South Atlantic convergence zone determine
125 Quito’s climate (Hastenrath, 1997; Vincenti et al., 2012; Zambrano-Barragán et al., 2011). Quito’s precipitation distribution
126 has two modalities, March–April and October–December, with an average annual precipitation of 1200 mm and an average
127 annual temperature of 13.4°C (Vincenti et al., 2012; Zambrano-Barragán et al., 2011). In recent decades, Quito’s urban
128 extent has spread many kilometres to the north, east, and south (Bonilla-Bedoya et al., 2020b; Salazar et al., 2020).
129 Westward expansion is limited, although not absent, due to the designated protected areas on the slopes of Pichincha
130 volcano, which were implemented following urban encroachment and the incidence of landslides and floods (Vidal et al.,
131 2015; DMQ, 2018). Urban expansion is changing Quito’s exposure to natural hazards including landslides, floods, volcanic
132 activity, and earthquakes (Chatelain et al., 1999; Hall et al., 2008; Carmin and Anguelovski, 2009; Valcárcel et al., 2017).
133 Quito’s urban area now exceeds the current Metropolitan District of Quito (DMQ) administrative boundary (Bonilla-Bedoya
134 et al., 2020a; Salazar et al., 2021). Therefore, in this study, we define two separate areas of interest (AOIs): (1) a ‘land cover
135 AOI’ for mapping land cover change, which encompasses the core urban area of Quito, and (2) a ‘city AOI’ for mapping

Deleted: , Ecuador

138 greenspace, which includes the Administrative Level 3 Parishes of Quito, Cumbaya, Llano Chico, Calderon (Carapungo),
 139 Conocoto, Zambiza, and Nayón (Fig. 2a, S1).

Deleted: o



140
 141 **Figure 2:** (a) The location of Quito, Ecuador in relation to regional seismic faults and volcanoes. Fault lines (red) are from the
 142 Geophysical Institute of the National Polytechnic School (IG-EPN) and Global Earthquake Model Global Active Faults (Styron,
 143 2019). (b) Urban change and population of Quito are mapped using Open Government data (<http://gobiernoabierto.quito.gob.ec/>).
 144 (c) Volcanic hazards from the IG-EPN et al. (2019) Pichincha Volcano hazard map. (d) Landslide susceptibility map (Stanley and

146 Kirschbaum, 2017) and observed landslide events (n=1,321) (2006–2017) (<http://gobiernoabierto.quito.gob.ec/>). (e) Observed
147 Hydrometeorological (n=1,574) and forest fire events (n=2,358) (2006–2017) (<http://gobiernoabierto.quito.gob.ec/>).

148
149 Quito is surrounded by active faults (Fig. 2a) and the Global Earthquake Model estimates (Pagani et al., 2018) at the regional
150 scale indicate a relatively high seismic hazard with a Peak Ground Acceleration (PGA) of 0.55–0.9 g (with a 10%
151 probability of exceedance in 50 years) (Fig. S1). Similarly, Beauval (2018) estimate a PGA of ~0.4–0.6 g for Quito in a
152 return period of 475 years. The Quito Fault System creates seismic hazard across the city, with a maximum earthquake size
153 estimated at M_w 6.6 and a recurrence time of ~150–435 years (Alvarado et al., 2014). Earthquake scenario damage models
154 show that the highest rates of potential building damage are associated with areas of highest social vulnerability (Valcárcel et
155 al., 2017). Volcanic eruptions also pose significant risk to large populations. Quito lies 12 km from the active volcano
156 Guagua Pichincha, where activity over the past decades has been characterised by small explosions, ash, and gas emission
157 (Loughlin et al., 2015). Past eruptions have covered Quito in ash, for example, the 1660 eruption ash deposits are ~10 cm
158 thick in central Quito (Robin et al., 2008). Recent pyroclastic flows and surges have been channelled by topography away
159 from Quito to the west, but potential volcanic hazards in Quito include secondary lahars as well as ashfall, which are mapped
160 using knowledge of historic eruptions (IG-EPN, 2019) (Fig. 2c). Quito's road network, and water supply, are also all
161 vulnerable to flows and especially ash from multiple volcanoes (Wilson et al., 2012; Loughlin et al., 2015). Landslides and
162 floods are both extensive natural hazards in Quito owing to the steep topography, intense rainfall, and filling of natural
163 drainage channels to create building space (DMQ, 2018; Castelo et al., 2018; Domínguez-Castro et al., 2018; Perrin et al.,
164 2001). Landslides are concentrated on the steep slopes of Quito's periphery and ravines (Fig. 2d), whereas flood events are
165 spread across Quito's urban extent (Fig. 2e). Following heavy rainfall, mudflows are also a hazard on the lower and
166 increasingly urbanised slopes of Pichincha (Perrin et al., 2001). Multi-hazards or cascading hazards could also emerge
167 through combinations of single hazards, such as a volcanic eruption that deposits ash on slopes and blocks urban drains,
168 which if followed by heavy rain could produce lahars and urban flooding respectively (Gill et al., 2021).

169
170 In terms of policy and planning, the issue of green space in the city currently maintains a spatial-functional emphasis,
171 although environmental (mainly related to climate change) and socio-political (public space, right to the city) criteria have
172 been incorporated. There was an important change in the first urban plan of the city (1942), where the design envisages a
173 series of green spaces, especially in the north of the city, under a criterion of recreational and sports spaces. This is the case
174 of the current La Carolina park, which was initially the city's racecourse. The plan also considered a series of smaller green
175 spaces within the residential areas. However, a balanced development between urban sprawl and the environment was not

176 planned, but rather green and open spaces in general were thought of as part of the zoning logic of the time. This model of
177 urban development between the 1970s and 2000s is the main risk factor for disasters in the city (Carrión and Erazo Espinosa,
178 2012). In 1993, the Metropolitan District of Quito (DMQ) was created, with 9.3% of its territory being urban and 90.7%

Moved (insertion) [1]

Deleted: Although less frequent, v

Deleted: and earthquakes

Field Code Changed

Moved up [1]: Although less frequent, volcanic eruptions and earthquakes pose significant risk to large populations. Quito lies 12 km from the active volcano Guagua Pichincha, where activity over the past decades has been characterised by small explosions, ash and gas emission (Loughlin et al., 2015). Past eruptions have covered Quito in ash, for example, the 1660 eruption ash deposits are ~10 cm thick in central Quito (Robin et al., 2008). Recent pyroclastic flows and surges have been channelled by topography away from Quito to the west, but potential volcanic hazards in Quito include secondary lahars as well as ashfall, which are mapped using knowledge of historic eruptions (IG-EPN, 2019) (Fig. 2c). Quito's road network and water supply, are also all vulnerable to flows and especially ash from multiple volcanoes (Wilson et al., 2012; Loughlin et al., 2015).

Deleted: The Global Earthquake Model estimates (Pagani et al., 2018) at the regional scale indicate a relatively high seismic hazard with a Peak Ground Acceleration (PGA) of 0.55–0.9 g (with a 10% probability of exceedance in 50 years) (Fig. S1). Similarly, Beauval (2018) estimate a PGA of ~0.4–0.6 g for Quito in a return period of 475 years. The Quito Fault System creates seismic hazard across the city, with a maximum earthquake size estimated at M_w 6.6 and a recurrence time of ~150–435 years (Alvarado et al., 2014). Earthquake scenario damage models show that the highest rates of potential building damage are associated with areas of highest social vulnerability (Valcárcel et al., 2017). ...

Deleted: urbanisation

208 rural. This new territorial configuration is relevant because both planning and risk analysis tend to concentrate only on the
209 urbanised area (Peralta Arias and Higuera García, 2016).

210
211 When outlining the vision of Quito to year 2040, the Municipality of the Metropolitan District of Quito recognised the
212 importance of an urban green network for delivering social and natural benefits, including risk mitigation (DMQ, 2018). This
213 recognition of greenspace to reduce risk from morphoclimatic events has been present in the planning instruments of the
214 Municipality since the 1980s. The destructive mudflows of 1983 on the slopes of Pichincha that had been previously
215 urbanised by informal settlements prompted the national government of Ecuador to legislate for the law on “protective
216 forests”. These forests were designed to prevent erosion, mitigate landslides, and control informal urbanisation on slopes
217 around Quito. According to Sierra (2009), the role of greenspace in the borders of the city were first designed as recreational
218 and patrimonial landscapes from 1940s onwards, and later, in the 1970s and 1980s incorporated environmental, city growth
219 control, and risk mitigation properties. In the last 30 years, there has been Municipal and community interest in the recovery
220 of ravines for recreational activities and improving citizens quality of life by implementing nature-based solutions alongside
221 urban development; however, its realisation and impact has been small at the city scale, instead confined to planning-stage
222 pilot projects such as in the San Enrique de Velasco district in the northwest of Quito (Salmon et al., 2021).

223
224 The following section details our methodology to quantify Quito’s historical urban growth and investigation of future urban
225 growth scenarios. We investigate Quito’s growth in conjunction with topographical information and hazard datasets to reveal
226 how Quito’s exposure to hazards is changing through time. We then define a methodology to map greenspace that is
227 potentially suitable for disaster risk reduction, considering the spatial distribution in relation to socioeconomic data, and per
228 person accessibility if the spaces were used as an emergency refuge. These data are then used to reveal optimum locations
229 for the designation of new protected greenspaces to enhance disaster risk resilience in Quito.

230 **3 Methodology**

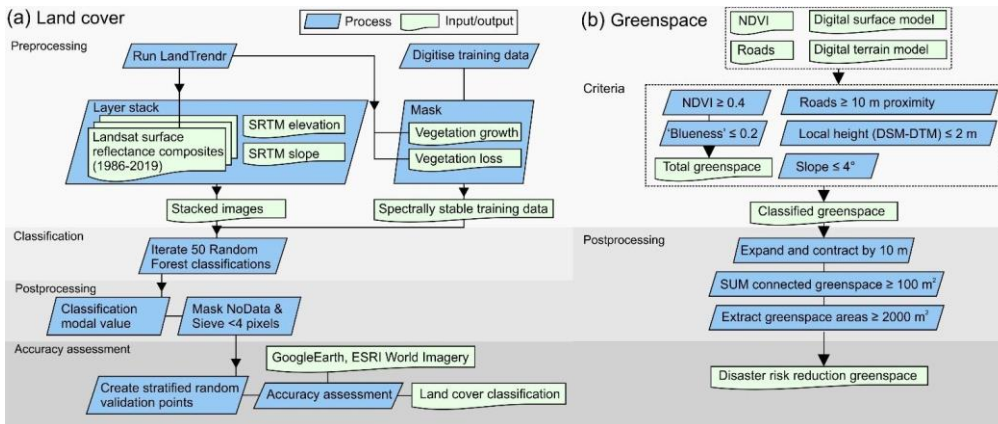
231 **3.1 Urban growth**

232 Urban growth for the period 1986 to 2020 was derived by applying a land cover classification workflow to 30 m resolution
233 Landsat satellite imagery for the Land Cover AOI (Fig. 2a, 3a), including Landsat 4 Thematic Mapper (TM), Landsat 7
234 Enhanced Thematic Mapper Plus (ETM+), and Landsat 8 Operational Land Imager (OLI). Landsat imagery was selected
235 June to September to avoid cloud cover during the wet season (Domínguez-Castro et al., 2018). Therefore, seasonal spectral
236 variations in land covers are not captured. Images were pre-processed using Landsat-based detection of Trends in
237 Disturbance and Recovery (LandTrendr) and Google Earth Engine to create multi-image mosaics with minimal cloud cover
238 using a medoid pixel composite (Gorelick et al., 2017; Kennedy et al., 2018). Training data were manually digitised as 500
239 polygons (median polygon area of 5,400 m²) with reference to the 1986 image using four classes: 1) urban, 2) woodland, 3)

240 scrub vegetation and bare ground, and 4) agriculture and grassland. Training data were masked using the normalised
241 difference vegetation index (NDVI) vegetation loss and growth masks that are output from LandTrendr to leave areas of
242 training data that were spectrally consistent through time (1986–2020). Landsat composites were stacked with elevation and
243 slope layers derived from the 30 m Shuttle Radar Topography Mission (SRTM) digital elevation model (DEM) (Farr et al.,
244 2007) since these additional variables were shown to improve land cover classification performance (Zhu et al., 2016). We
245 used a Random Forest classification, which is a decision tree approach popular for land cover classifications owing to their
246 high accuracy, broad data handling, and low sensitivity to training data noise (Rodríguez-Galiano et al., 2012; Zhu et al.,
247 2016). The Orfeo Toolbox Random Forest classifier (Inglada and Christophe, 2009) (Table S1) was run 50 times for each
248 time period using 200 trees and a random sample of training data to account for imbalance between classes (Millard and
249 Richardson, 2015) (Table S1). The modal value was used to produce the final classification map, which was accuracy
250 assessed using an independent stratified random sample of 200 reference points in each class created using high resolution
251 satellite imagery (Fig. S2). High resolution multispectral satellite imagery was not available in the 1980s, which reduces
252 classification confidence in training and reference data, however, a panchromatic ~1 m resolution aerial orthophoto of Quito
253 in 1977 from Instituto Geográfico Militar (1977) was used for reference. The accuracy assessment was used to produce an
254 error-adjusted area and confidence interval of each land cover classification (e.g. Olofsson et al., 2013; Olofsson et al.,
255 2014).

256
257 Future urbanisation scenarios in Quito were assessed with reference to Bonilla-Bedoya et al. (2020b) and Salazar et al.
258 (2020). Both studies used predictor variables to model future urbanisation scenarios in Quito. Salazar et al. (2020) present a
259 scenario to the year 2050, whereas Bonilla-Bedoya et al. (2020b) define an ‘urbanisation probability’ without a scenario end
260 date. Nonetheless, the spatial trends in both studies are similar. Predictors used to derive urbanisation probability included
261 biophysical (e.g. precipitation, slope, and altitude), land cover and management (e.g. protected areas), infrastructure and
262 services (e.g. road network), socioeconomic (e.g. land value), and landscape metrics (e.g. landscape patch size and shape)
263 (Bonilla-Bedoya et al., 2020). We used ‘high’ (urbanisation probability: 55–79 %) and ‘very high’ (urbanisation probability:
264 79–100 %) classes from Bonilla-Bedoya et al. (2020b) in this study (Fig. S3) to evaluate future land cover scenarios and the
265 intersection of urban areas with hazards.

266



267
268 **Figure 3: (a) Land cover classification and accuracy assessment workflow. (b) Classification of greenspace that could potentially**
269 **contribute to disaster risk reduction (DRR), herein 'DRR greenspace'.**

270 **3.2 Topography**

271 The 30 m SRTM DEM was used to extract statistics on the elevation and slope within the land cover change area of interest
272 (AOI), which encompasses the smaller city AOI (Fig. 2a). A higher resolution (2 m and 10 m) DEM and orthoimagery was
273 created for a smaller AOI (Fig. 2a), which bounded the Administrative Level 3 Parishes of Quito, Cumbaya, Llano Chico,
274 Calderon (Carapungo), Conocoto, Zambiza, and Nayon. This AOI was covered by tristereo Pleiades imagery, which were
275 acquired on five separate dates (5th November 2019, 28th January 2020, 9th February 2020, 6th June 2020, and 28th July 2020)
276 in both panchromatic (~0.7 m) and multi-spectral (~2.8 m RGB and Near Infrared) modes (Table S2). Tristereo acquisitions
277 produce elevation models with lower uncertainties compared to bistereo acquisitions due to greater point cloud densities
278 afforded by the extra viewing angle (Zhou et al., 2015). All imagery was delivered with radiometric processing to reflectance
279 and processed using rational polynomial coefficients (RPCs) without ground control points (GCPs) (e.g. Airbus Defence and
280 Space, 2012; Zhou et al., 2015). Agisoft Metashape v.1.6.5 was used to process the imagery to create a DEM, digital terrain
281 model (DTM), and orthorectified imagery. Briefly: (1) the panchromatic and multispectral imagery were aligned in one
282 bundle to produce a sparse point cloud; (2) the sparse cloud was filtered to remove outliers using Metashape's gradual
283 selection tools; (3) a dense point cloud was constructed using the panchromatic imagery, which was used to create a 2 m
284 resolution DEM and (4) orthorectify the satellite imagery. Metashape's ground classification (maximum angle: 15°,
285 maximum distance: 0.5 m, cell size: 50 m) was applied to the dense cloud and used to create the DTM. An additional DSM
286 was output at 10 m resolution to reduce data gaps for deriving a Topographic Wetness Index (TWI) (Section 3.3).
287

Deleted: supplied

Deleted: with

290 ~~Since the~~ Pleiades DEM was ~~processed without GCPs, we assessed the accuracy~~ using Ice, Cloud and land Elevation
291 Satellite (ICESAT-2) altimetry data. ICESAT-2 data has an expected vertical accuracy that is lower than the error expected
292 from a Pleiades DEM created without ground control points ($> 3\text{--}5\text{m}$) (Passalacqua et al., 2015; Markus et al., 2017) and
293 was therefore used as an independent validation check. We extracted High Confidence returns from the Advanced
294 Topographic Laser Altimeter System (ATLAS) instrument ATL03 Global Geolocated Photon Height data acquired 6th
295 December 2018 to 3rd June 2020 that intersected with the Pleiades data (Neumann et al., 2019; Neumann et al., 2020).
296 Photons were filtered to exclude slopes steeper than 20° and aggregated into 5 m grid cell mean values. Cells containing ≥ 2
297 photons with an elevation range ≤ 1 m, were carried forward for the validation ($n = 11,922$). We coregistered the Pleiades
298 DEM and gridded ICESAT-2 data following the x, y, z shift correction of Nuth and Käab (2011) and the difference in
299 elevation values were compared. The mean vertical difference between the ICESAT-2 and Pleiades data was 0.38 m (one
300 standard deviation: 1.32 m) with a normalised median absolute deviation of 0.84 m.

Deleted: The accuracy of the

Deleted: assessed

301 3.3 Hazards

302 Information on natural hazards affecting Quito were collated from published sources and Ecuador's Open Government data.
303 We used a global landslide susceptibility model that was validated against local and global landslide inventories, with an
304 emphasis on rainfall-triggered events (Kirschbaum et al., 2016; Stanley and Kirschbaum, 2017). Landslide susceptibility was
305 ranked on a scale of 1 (low) to 5 (high) and the model combined data on slope, faults, geology, forest loss, and road
306 networks, aggregated to ~ 1 km grid cells (Stanley and Kirschbaum, 2017). Open Government records of 'Accidents' 2006–
307 2017 were used to identify the geographic distribution of mass movement events ($n = 1,321$), which were compared to the
308 global landslide susceptibility model (Fig. S4) (Ministry of Territory, Habitat and Housing., 2020). We masked Class 5
309 (high) of the landslide susceptibility model out of the future urbanisation scenario of Bonilla-Bedoya et al. (2020b) to create
310 a restricted scenario of urban growth, which reflects DMQ's vision to remove high risk areas from future land occupation.
311 We also excluded development on the slopes of Pichincha volcano (as unrealistically inaccessible given steep slopes) and
312 included an area of development spanning the Metropolitan District boundary in the south (Fig. S3). We refer to the original
313 scenario of future urbanisation and the modified scenario as F-U and M-U respectively. Information on volcanic hazards
314 were obtained from the Geophysical Institute of the National Polytechnic School (IG-EPN) through the National Information
315 System (SNI) (SNI, 2020). Spatial variation in earthquake hazard across Quito was not explored in this study due to the
316 coarse resolution (~ 10 km) of available hazard information (Fig. S1). However, the high regional seismic hazard (Alvarado
317 et al., 2014; Pagani et al., 2018) motivates our city-wide analysis of greenspace.

318
319 The 10 m Pleiades DEM was hydrologically corrected by breaching sinks (Lidberg et al., 2017), using the *Breach*
320 *depressions least cost tool* of Whitebox 1.4.0. The breached DEM was used to derive a TWI, which was intersected with
321 flood events in the Open Government database ($n = 1,274$) to assess whether high TWI values correspond to greater

324 incidences of flood events, and therefore was indicative of potential flood hazard (Jalayer et al., 2014; Kelleher and
325 McPhillips, 2020).

$$326 \quad TWI = \ln \left(\frac{a}{\tan \beta} \right) \quad (1)$$

328
329 where a represents the specific catchment area and $\tan \beta$ represents the local DEM slope. Therefore, the TWI describes the
330 tendency for a cell to accumulate and evacuate water (Beven and Kirkby, 1979; Manfreda et al., 2011; Mattivi et al., 2019).
331 We assumed a positional uncertainty radius of 20 m in the flood event records based on the observed positional spread of
332 recorded traffic collisions at road junctions in the same database (Fig. S5). The maximum TWI value within a 20 m radius of
333 the recorded point was extracted and compared to the TWI for a random sample of 10,000 points to test whether there was a
334 statistically significant difference in the TWI at locations of flood events (e.g. Kelleher and McPhillips, 2020). Notably, this
335 method does not account for the subsurface drainage network present in an urban setting, and therefore represents an
336 assumption that this subsurface drainage network is overwhelmed during the flood event, such that all flow passes over the
337 DEM (Kelleher and McPhillips, 2020).

339 3.4 Greenspace

340 Orthorectified multi-spectral Pleiades imagery was pansharpened in ArcGIS Pro 2.6.0 using the Gram-Schmidt algorithm
341 and Pleiades sensor band weights to create a four-band (red, green, blue, and near infrared (NIR)) 0.5 m resolution multi-
342 spectral image. Quito's vegetated greenspace distribution was mapped using the NDVI applied to the NIR and red bands of
343 the pansharpened Pleiades satellite imagery (Fig. 3b):

$$344 \quad NDVI = \frac{(NIR - Red)}{(NIR + Red)} \quad (2)$$

346 Negative NDVI values correspond to areas lacking vegetation, whereas increasingly positive values represent healthy
347 vegetation (Tucker et al., 1981; Pettorelli et al., 2005). In some cases, shadowed areas, for example due to buildings, display
348 similar NDVI values to vegetation (Leblon et al., 1996; Yamazaki et al., 2009). We therefore used 100 randomly sample
349 patches (200×200 m) to evaluate the NDVI classification with reference to the pansharpened Pleiades orthoimage. Incorrect
350 classifications had a small overall impact, accounting for 0.4 % of the evaluated NDVI area (Table S3) with a mean patch
351 size of 13±16 m². Bright blue roofs also displayed a high NDVI value and were masked out using a simple 'blueness' index
352 of values ≤ 0.2 , which was derived through manual inspection of blue roofs:

$$353 \quad Blueness = 2 \times Blue - Red - Green \quad (3)$$

Formatted: Superscript

355

356 Whilst global coverage and daily observation is possible with the paired constellation, Pleiades imagery is not routinely
357 acquired nor open access. Therefore, we also compared Pleiades NDVI values with those from an open access Sentinel-2
358 image acquired 6th February 2020 with the aim of testing their consistency, noting that whilst the spectral bands overlap, the
359 bandwidth of Pleiades is greater (Pleiades: red 590–710 nm, NIR 740–940 nm, Sentinel-2: red 649–680 nm, NIR 780–886
360 nm).

361 3.4.1 Disaster risk reduction (DRR) greenspace

362 Greenspaces potentially suitable for providing safe spaces and contributing towards disaster risk reduction were identified
363 using an EO-based workflow (Fig.3b) for areas within 800 m (accessible within a ~10-minute walk) (e.g. Dou and Zhan,
364 2011; Jeong et al., 2021) of populations in Quito’s urban extent. The workflow identified greenspace: (1) that is vegetated,
365 (2) greater than 10 m from a road to exclude road verges; (3) with slope $\leq 4^\circ$ to provide a suitable gradient for ‘safe spaces’
366 (Kilci et al., 2015; Liu et al., 2011); and (4) with a local height (≤ 2 m) to identify open ground and exclude raised vegetation
367 such as trees. Expansion and contraction buffers of 10 m were applied to connect adjacent patches of greenspace into
368 greenspace ‘zones’, which for example could represent multiple patches of classified greenspace within a park. All areas of
369 greenspace with a patch size ≥ 100 m² within these zones were summed and zones totalling ≥ 2000 m² of greenspace were
370 classified as ‘potential DRR greenspace’. Space requirements in a disaster situation are dynamic; however, a 100 m² patch
371 size is recommended to accommodate two people with communal space (cooking, access, facilities etc) in a camp-style
372 settlement following guidelines in the Sphere Humanitarian Charter and Minimum Standards in Humanitarian Response
373 Handbook (Anhorn and Khazai, 2015; Sphere Association, 2018). Zones of 2000 m² approximate one quarter to one third of
374 a professional football pitch so could be expected to already exist as functional greenspaces (e.g. recreation parks) in an
375 urban environment. These spaces were evaluated alongside a list of safe spaces designated by DMQ for use in an earthquake
376 event (Metro Ecuador, 2019)(Table S4), in conjunction with population data projected to 2019 and socioeconomic
377 classification data (Instituto Geográfico Militar, 2019). These socioeconomic classifications characterise a continuum of
378 education, income, and lifestyle factors into five classes, ranging from ‘high’ to ‘low’, where ‘low’ represents basic
379 education and limited household facilities such as rubbish collection and plumbing, whereas ‘high’ represents higher
380 education, and houses or apartments that are provisioned with state services (Instituto Geográfico Militar, 2019).

381 3.4.2 Greenspace capacity

382 Quito’s 2019 population data (Instituto Geográfico Militar, 2019) were used to assess the population capacity of all DRR
383 greenspace (3.4.1) in the event that they were to be used for accommodation following a disaster such as an earthquake. We
384 assessed the capacity of two types of greenspaces: (1) DRR greenspace that overlapped with DMQ designated greenspaces,
385 which included city parks and safe spaces (3.4.1), and (2) all DRR greenspaces identified in this study that were either
386 designated or undesignated. These two scenarios therefore represent the DRR capacity based on current designations (1),

Deleted: S3

Deleted: classes

389 compared to the potential maximum capacity (2). We considered two separate cases of populations within 800 m and 1600 m
390 network buffers of each greenspace. For each scenario, we used a network analysis to assign population demand points to
391 each greenspace based on their proximity, up to the maximum buffer distance. The network was constructed as a grid at 100
392 m resolution and considered population demand points also gridded at 100 m resolution, which were uniformly
393 disaggregated from census polygons. The number of people that could be accommodated in each greenspace depends on the
394 capacity of the space, and the population demand in the surrounding buffer. We considered capacities based on Sphere
395 Association (2018) guidelines, which suggest an allocation of 45 m² per person (recommended amount per person
396 accounting for communal facilities and infrastructure in an emergency shelter setting) and 3 m² per person (minimum living
397 space per person). All demand within the buffers was allocated to the closest greenspaces, therefore excess demand was
398 reported as overcapacity. We did not consider the possibility of people moving greater distances around the city to distribute
399 the population demand more equally, which could occur following an initial disaster situation, or that only a fraction of the
400 population would require access to refuge space in a disaster situation. Considering potential policy consideration, we also
401 used a maximum capacitated coverage network analysis (e.g. Anhorn and Khazai, 2015) with the same datasets to find the
402 'top ten' DRR greenspaces in Quito based on a minimum space requirement of 3 m² per person and a travel distance of 800
403 m.

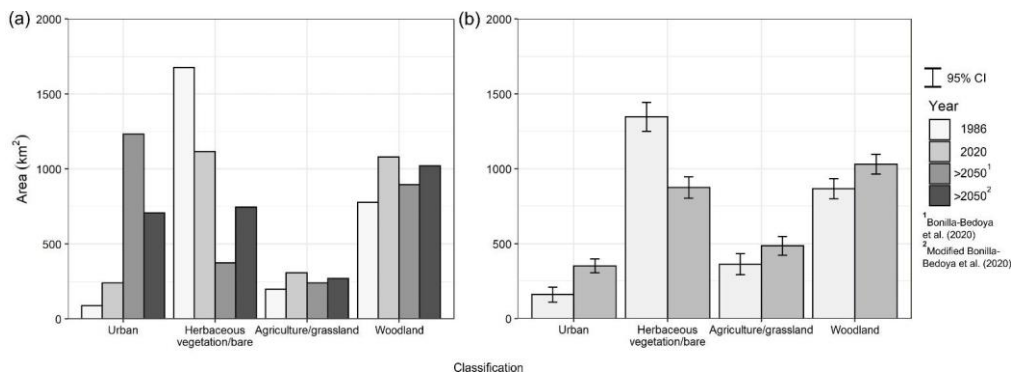
404 **4 Results**

405 **4.1 Urban growth**

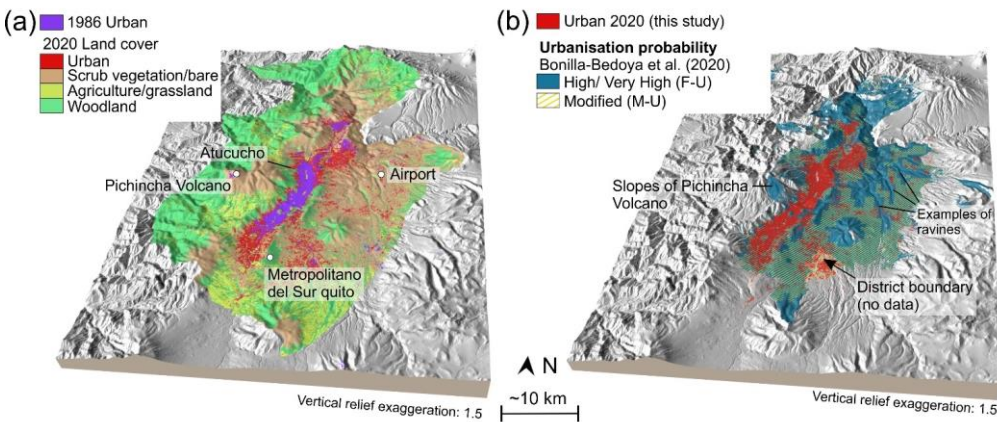
406 Our land cover classifications showed that the urban area of Quito expanded ~192 km² over the study period, more than
407 doubling from 160±50 km² in 1986 to 352±47 km² in 2020 (Fig. 4, Table [S5](#)). Urban expansion was primarily aligned along-
408 valley (north south) and eastward (Fig. 5a), into areas of previously scrub vegetation/bare and agricultural/grassland classes.
409 The future urbanisation scenario of Bonilla-Bedoya et al. (2020b) covered an urban area of 1,232 km² (F-U), whereas the M-
410 U scenario covered 705 km² (Fig. 4a), which was still double the observed 2020 urban area. Future urbanisation in the
411 modelled scenarios was predominantly eastward, where lower density urbanisation interspersed with the scrub
412 vegetation/bare ground class was already apparent in 2020 (Fig. 5). The area of woodland and agriculture/grassland classes
413 also increased 1986–2020. A notable example of afforestation (4.8 km²) was the park Metropolitano del Sur, which is
414 located on the southeast of the city limit (Fig. 5a).

415

Deleted: S4



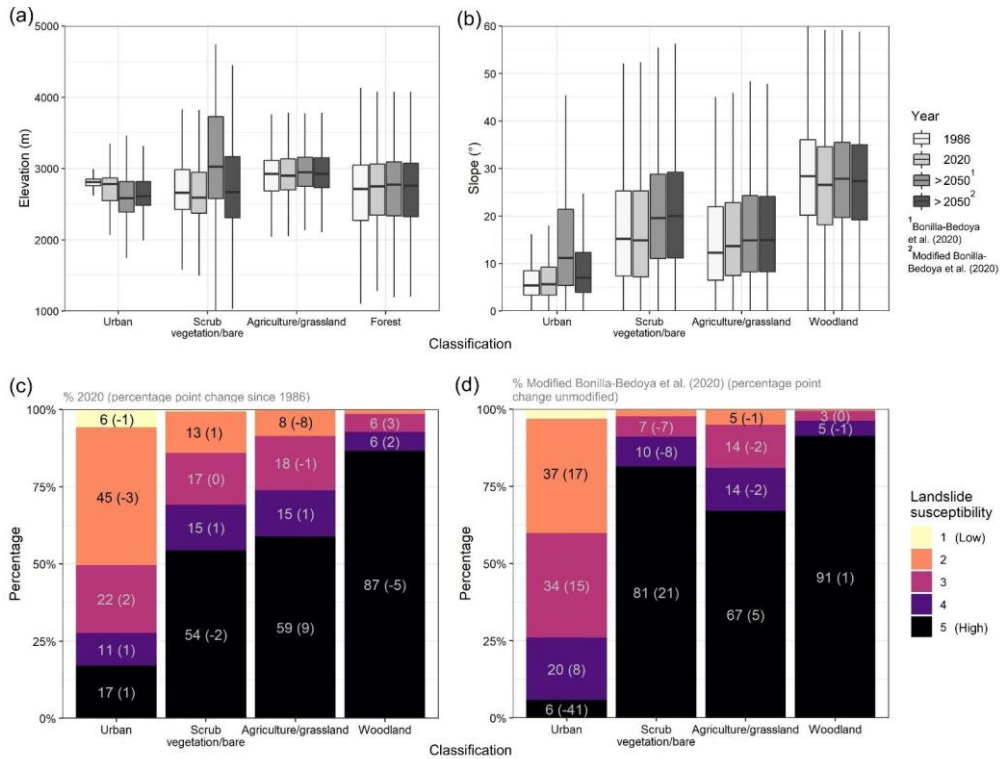
417
 418 **Figure 4: (a) Mapped land cover classification results for 1986 and 2020 alongside modelled future land cover from two scenarios^(1, 2)**
 419 **using data from Bonilla-Bedoya et al. (2020). (b) Error-adjusted (e.g. Olofsson et al., 2013; Olofsson et al., 2014) land cover**
 420 **classification results from 1986 and 2020.**



423
 424 **Figure 5: (a) 3D perspective showing urban growth 1986–2020 and land cover. (b) Quito's urban area in 2020 compared to modelled future urbanisation (F-U)**
 425 **(Bonilla-Bedoya et al., 2020) and a modified scenario (M-U). Background is a hillshaded**
 426 **SRTM DEM.**

427 The median elevation of Quito's urban extent in 2020 (2,780 m) was similar to 1986 (2,810 m); however, the city covered a
 428 broader elevation range in 2020, tending towards lower elevations (Fig. 6a), which was also apparent for the F-U and M-U
 429 scenarios. The urban class displayed the smallest spread of values for topographic slope (Fig. 6b). Here, the median slope of

430 the urban class was $\sim 5^\circ$ in 1986 and 2020, however this increased to 11° and 7° in the F-U and M-U scenarios respectively,
 431 in addition to a broader spread of slope values. Woodland featured the highest median slope of all land cover classes ($\sim 28^\circ$)
 432 and a comparable median elevation to the urban class ($\sim 2700\text{--}2800$ m).
 433



434
 435 **Figure 6: Elevation (a) and slope (b) characteristics of the classified and modelled land cover scenarios. Boxes show the**
 436 **interquartile range and the median (horizontal line). Lines show values within 1.5 times the interquartile range. Outliers are not**
 437 **shown. (c) 2020 land cover intersections with landslide susceptibility and the percentage points change since 1986. (d) Future land**
 438 **cover intersections with landslide susceptibility using modified urbanisation probability (M-U) of Bonilla-Bedoya et al. (2020, and**
 439 **the difference compared to the unmodified scenario (F-U).**

440 4.2 Intersection with hazards

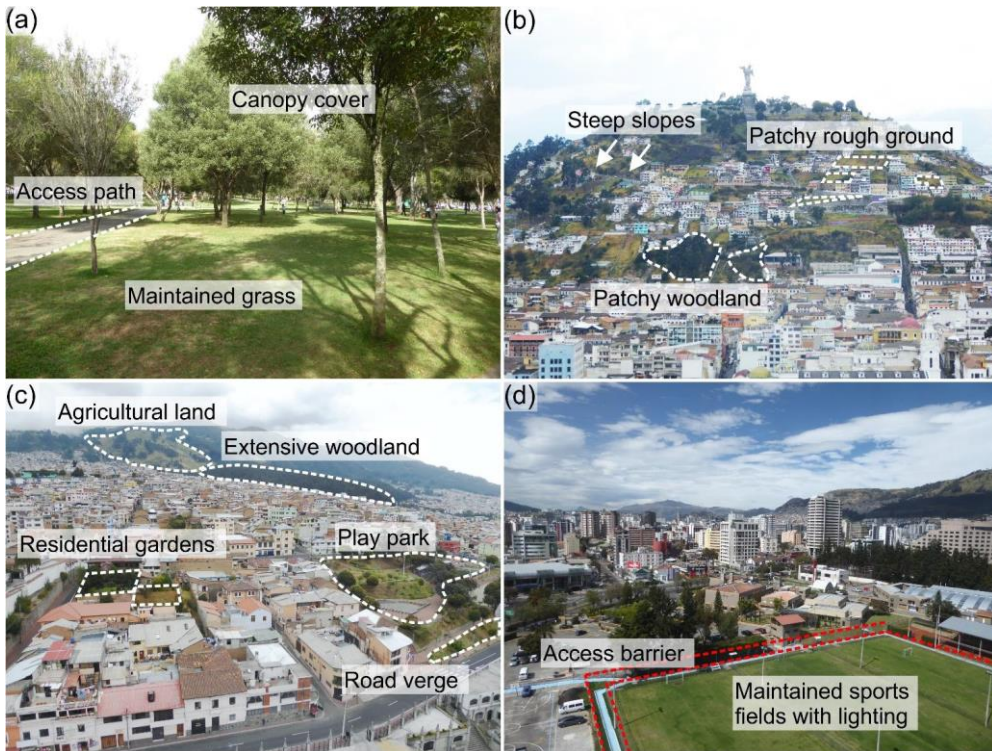
441 Landslides are one of the most common natural hazards in Quito (DMQ, 2018). We found good spatial association between
 442 observations of landslide events in Ecuador's Open Government database (2006–2017) and a landslide susceptibility model

443 (Stanley and Kirschbaum, 2017) (Fig. S4). Of 1,321 recorded events, 82% (n = 1,089) fell within landslide susceptibility
444 categories 3–5, of which 44% (n = 576) were in the highest category (5). Ten events were observed in the lowest category
445 (1). We observed a small change in the landslide susceptibility of the urban class 1986–2020. Here, the urban area in the
446 highest landslide susceptibility categories (4 and 5) increased by 2 percentage points 1986–2020 (Fig. 6c). The largest
447 change was observed in the agriculture/grassland class, which featured a 9-percentage point increase in category 5 (high)
448 landslide susceptibility. Woodland mostly occurred within the highest landslide susceptibility category 5 (87%) (Fig 6c).
449 Regarding future urbanisation, the M-U scenario restricted future urbanisation in landslide susceptibility category 5,
450 therefore the observed percentage of urban area in category 5 (6%) was notably lower than in the F-U scenario (47%), which
451 did not enforce any restrictions.

452
453 Flood events in Quito that were recorded in Ecuador’s Open Government database were evaluated alongside a TWI derived
454 from the 10 m resolution Pleiades DEM, [noting that this does not account for subsurface drainage](#). Median TWI values for
455 all flood events (n = 1,274), clustered flood events where two or more events were located within 40 m of each other (n =
456 125), and a random sample (n = 10,000), were 13.3, 14.4, and 12.1 respectively (Fig. S6). Clustered flood events, which
457 displayed the highest TWI, could correspond to areas of nuisance flooding since multiple events are located in close
458 proximity (Kelleher and McPhillips, 2020). Two sample independent Welch t-tests (one-tailed) showed that the difference in
459 TWI values between all flood events and clustered floods events were statistically significantly different from the random
460 sample ($p < 0.05$). Therefore, the mean TWI value was observed to be larger in areas of flood locations compared to the
461 random sample.

462 4.3 Greenspace

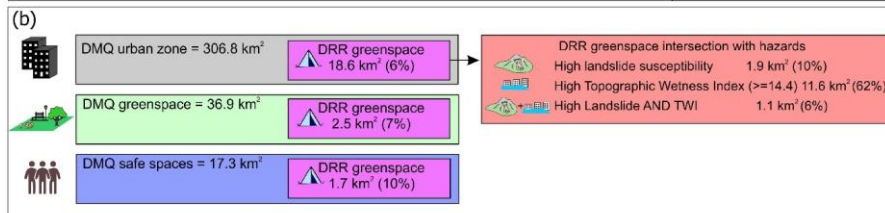
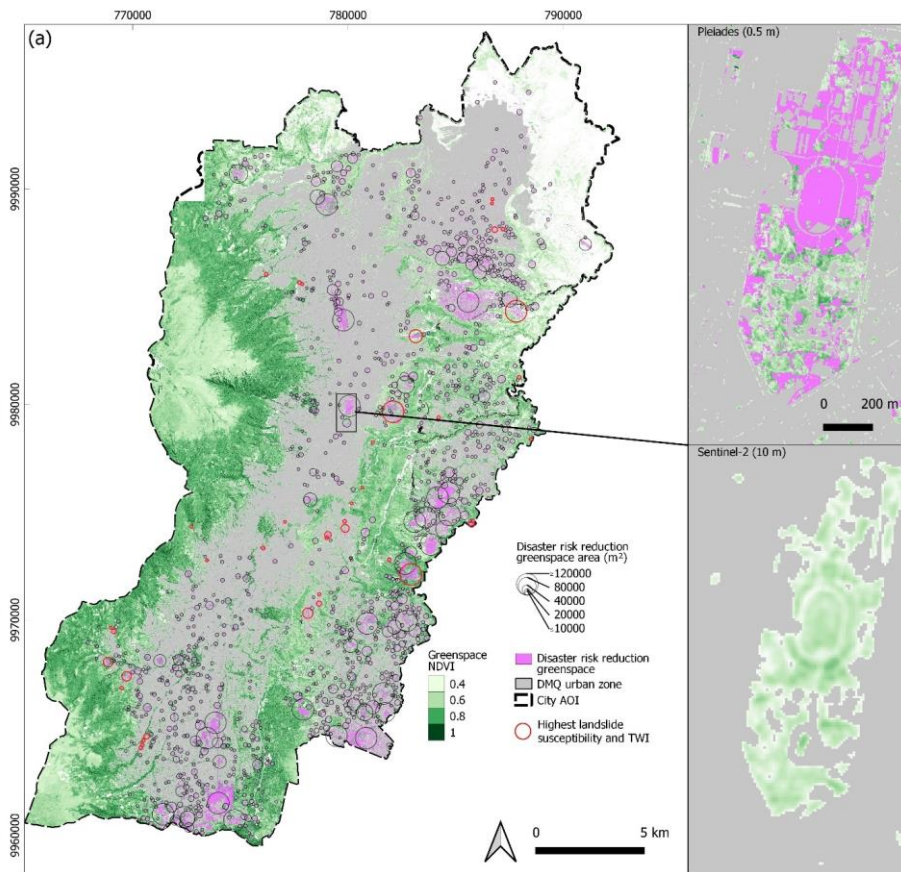
463 Quito includes multiple types of greenspace that provide ecological, social, and disaster risk reduction benefits (Fig. 1a, 7).
464 Within our AOI, 18.6 km² of potential DRR greenspace was identified, which covered 6% of the urban zone (Fig. 8). DMQ
465 designated greenspace had an area of 36.9 km², of which 2.5 km² (7%) intersected with potential DRR greenspace. Similarly,
466 DMQ designated safe spaces covered 17.3 km², of which 1.7 km² (10%) intersected with potential DRR greenspace.
467 Comparing DRR greenspaces with hazard information revealed that 62% of DRR greenspace intersected with areas of high
468 TWI values (≥ 14.4 (median value for clustered flood events - Section 4.2)), 10% intersected with areas of high (category 5)
469 landslide susceptibility, and 6% intersected with both hazards (Fig. 8b).



470

471

Figure 7: Examples of greenspace in Quito from photographs taken in October 2019 (a-d).



473 **Figure 8: Greenspace mapped using the NDVI applied to Pleiades satellite imagery shown with classified potential DRR**
474 **greenspace (black and red circles, pink shading). Red circles indicate DRR greenspace that intersects with landslide susceptibility**
475 **class 5 (high) and a Topographic Wetness Index value of ≥ 14.4 (median value for clustered flood events - Section 4.2). The inset of**
476 **Carolina Park shows the similarity of Pleiades-derived greenspace compared to greenspace mapped using Sentinel-2 imagery. The**
477 **Pleiades inset shows the distribution of potential DRR greenspace (pink) in Carolina Park. (b) Summary of greenspace availability**
478 **and hazard intersections.**

479 The association between population, socioeconomic classification (Instituto Geográfico Militar, 2019), and greenspace
480 accessibility was investigated for greenspaces ≥ 2000 m². The number of people living within close proximity to designated
481 greenspace was higher than for DRR greenspace (Fig. 9a). For example, 2.3 million (98%) of Quito's population were within
482 800 m of a designated greenspace, compared to 2.1 million for the DRR greenspace (88%). Distance to the nearest
483 greenspace was greater for 'low' and 'medium low' socioeconomic classifications compared to 'high' and 'medium high'
484 (Fig. 9b). Here, the difference in median values was greatest for designated greenspace (466 m), compared to our
485 classification of DRR greenspace (80 m). The amount of designated greenspace per person was smaller for lower
486 socioeconomic classifications, with a median of 3 m² per person for the 'low' classification compared to 8 m² for 'high'.
487 However, the amount of DRR greenspace was greatest for lower socioeconomic classifications, with a median of 24 m² per
488 person for 'low' compared to 4 m² for 'high' (Fig. 9c). This reflects lower population densities on the city margins (Fig. 9d)
489 and the persistence of agricultural land and undeveloped ground in these areas following urbanisation.

Deleted: living

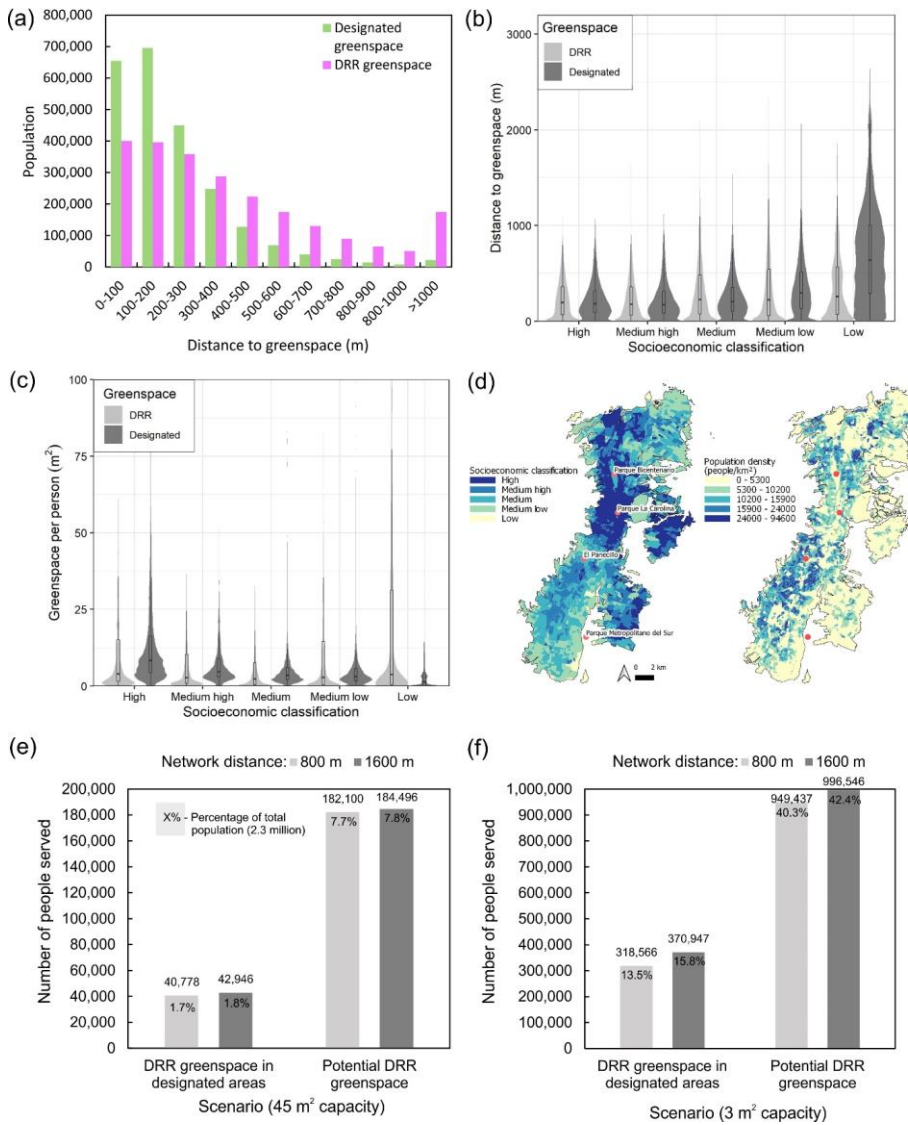


Figure 9: (a) Population proximity to designated and DRR greenspace. (b) Violin plot showing distance to the nearest greenspace for each socioeconomic classification. Overlaid boxplots show the interquartile range and the median (horizontal line). Lines show

Deleted: D

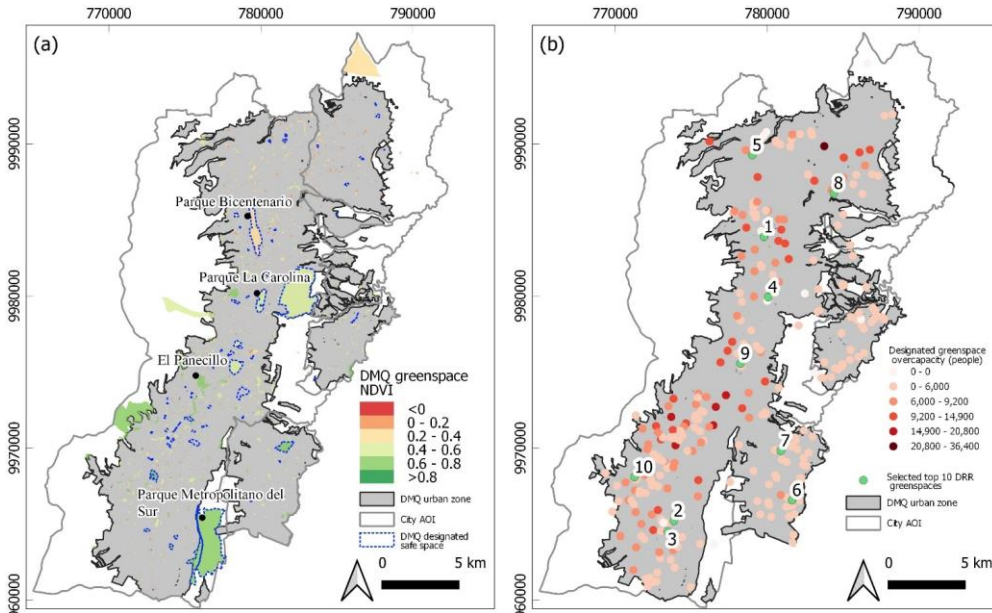
Deleted: Boxes

496 values within 1.5 times the interquartile range. Outliers are **excluded**. (c) **Violin plot showing greenspace per person within 800 m**
 497 **for each socioeconomic classification. Boxplots are overlaid with outliers excluded and values > 100 m² per person are not shown.**
 498 (d) Spatial variation in socioeconomic classification and population density for Quito using data from Instituto Geográfico Militar
 499 (2019). (e) Number of people that could be accommodated in DRR greenspace based on an allocation of 45 m² per person capacity
 500 and (f) 3 m² per person capacity. (e-f) Show capacitated populations for a network distance of 800 m (light grey bars) and 1600 m
 501 (dark grey bars) from the greenspace centroid and for DRR greenspace in designated spaces compared to all potential DRR
 502 greenspace mapped in this study.

503 **4.3.1 Greenspace capacity**

504 We assessed the capacity of each space considering the surrounding population demand. For populations within 800 m, DRR
 505 greenspace in currently designated areas could accommodate 1.7% (40,778) of Quito's population (total 2.3 million) with an
 506 allocation of 45 m² per person, or 13.5% (318,556) with 3 m² per person (Fig. 9 e-f, 10a). Considering all potential DRR
 507 greenspace (Fig. 8a), these values are 7.7% and 40.3% respectively (Fig. 9e-f). The top ten DRR providing greenspaces are
 508 shown in Fig. 10b and Fig. 11. Eight of these spaces overlap fully or partially with currently designated greenspaces or safe
 509 spaces and two did not (Fig. 11). Of these 278 currently designated spaces, only 10 were not over capacity based on the
 510 population demand (Fig. 10b).

511



512

Deleted: shown as black markers with transparen

Deleted: cy

Deleted: Outliers beyond the y-axis range (c) were excluded

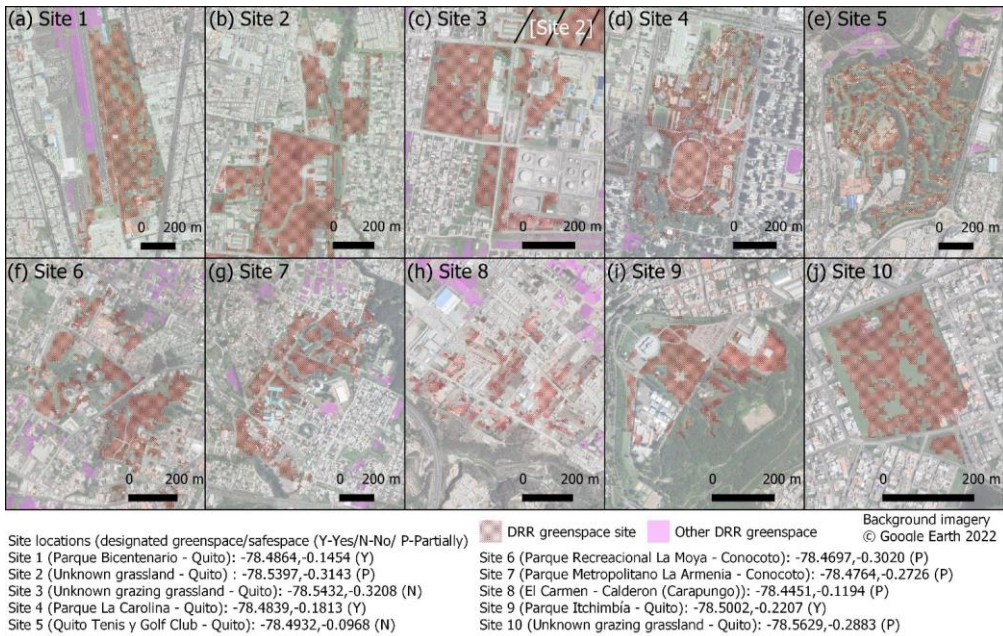
Deleted: G

Formatted: Superscript

Deleted: Figure

Deleted: Figure

519 **Figure 10:** (a) Designated green areas and safe spaces (blue dashed polygons) from Open Government data and their mean NDVI
 520 extracted using Pleiades satellite data. (b) Overcapacity of DRR greenspace in currently designated greenspaces or safe spaces.
 521 Green markers show the top 10 DRR greenspaces based on a maximum capacitated coverage model.
 522



523 **Figure 11.** Top ten ranked DRR greenspaces (red) and other nearby DRR greenspaces (pink) derived using a maximum
 524 capacitated coverage network analysis, which finds the greenspaces capable of accommodating the most people within 800 m using
 525 a minimum space requirement of 3 m² per person (Section 3.4.2).
 526

Deleted: .

527 5 Discussion

528 5.1 Urban growth and hazard intersections

529 Quito's historical urban expansion is largely aligned north-south, whereas future urban expansion is focussed to the north
 530 and east (Fig.5). Our study captures a period of land occupations starting in the 1980s including the settlement of Atucucho
 531 (Fig. 2b. [5a](#)), which formed informally in 1988 (Testori, 2016). This occupation is visible in our land cover classification
 532 (Fig. 5a). The formation date is labelled as 2003 in Open Government data (Fig. 2b), which likely reflects its origins as an
 533 informal settlement that was potentially not included in official maps until 2003. In this case, satellite imagery can capture

535 the urban sprawl of a city, including occupations that may not be apparent in historical maps. However, image classification
536 methods usually only capture 2D sprawl, and not vertical high-rise developments or redevelopments that are important for
537 measuring exposure to natural hazards (e.g. Amey et al., 2021). Quito's past and projected urban growth has been studied by
538 several authors in recent years (e.g. Bonilla-Bedoya et al., 2020b; Salazar et al., 2020; Valencia et al., 2020). Cross-
539 comparisons are complicated by the use of different study areas since Quito's urban area now exceeds the designated
540 metropolitan district boundary, which has prompted investigations to create a new district area (Salazar et al., 2021). By
541 comparing our urban classification (year 2020) to that of Bonilla-Bedoya et al. (2020) (year 2016) within the same area of
542 interest, we find urban areas of 213 km² and 210 km² respectively, which indicates classification consistency using EO data
543 despite different methodological approaches.

544
545 We observed that expansion of Quito and future projections tend towards lower elevations (Fig. 6a) and steeper slopes (Fig
546 6b), the latter of which is associated with encroachment into areas of high landslide susceptibility (Fig. 6c, d). Limited urban
547 expansion to the east of Quito on the steep slopes of Pichincha volcano suggests that a programme of protection to avoid
548 encroachment is working (Vidal et al. 2015). However, several of these areas or their vicinities are inhabited because of
549 previous land invasion dynamics that affected the peripheral green belt. They can be characterised from a spatial and
550 socioeconomic approach as a homogeneous space, in which the less economically favoured classes experience greater
551 possibilities of isolation from other social groups (Bonilla-Bedoya et al., 2020a). Further limiting eastward urban growth
552 reduces the ashfall and lahar hazard in the event of an eruption (Fig. 2c) and the hazard posed by landslides (Fig. 2d).
553 Additionally, the predominantly woodland slopes east of Quito (Fig. 5a) featured the highest landslide susceptibility scores
554 (87% of woodland is in class 5 (High) (Fig. 6c)) and are therefore a valuable target for protection against urbanisation. Our
555 observed decreasing elevation trend of Quito's urban area (Fig. 6a) reflects north-south and eastward expansion into lower
556 lying flatter areas, such that at a city-scale, Quito's landslide susceptibility did not notably increase 1986–2020 (Fig. 6c).
557 These areas are also the location of projected future expansion (Bonilla-Bedoya et al., 2020b; Salazar et al., 2020; Valencia
558 et al., 2020), predominantly through conversion of scrub vegetation and bare ground (Fig. 5a). Notable ravines exist in these
559 areas, therefore risk-informed planning to reduce encroachment on steep slopes, which was reflected in our M-U future
560 urban scenario, is desirable to minimise landslide risk to future developments. These areas are also likely to be most
561 susceptible to multi-hazards such as rainfall triggered lahar remobilisation or landslides, and flood and earthquake triggered
562 landslides (Gill and Malamud, 2017). Similarly, the filling of ravines from the seventeenth century onwards restricts the
563 drainage capacity during intensive rainfall and increases flood risk (Aragundi et al., 2016), therefore, incorporating
564 additional DRR greenspaces here to attenuate runoff and store water could be beneficial.

565
566 While risk-informed urbanisation can mitigate some hazards such as landslides, an intensive earthquake hazard exists in
567 Quito (Fig. S1), such that urban risk reduction requires building resilience at community to city-wide levels (Alvarado et al.,
568 2014; Valcárcel et al., 2017). A key element of resilience is the access to 'safe spaces' following an earthquake event where

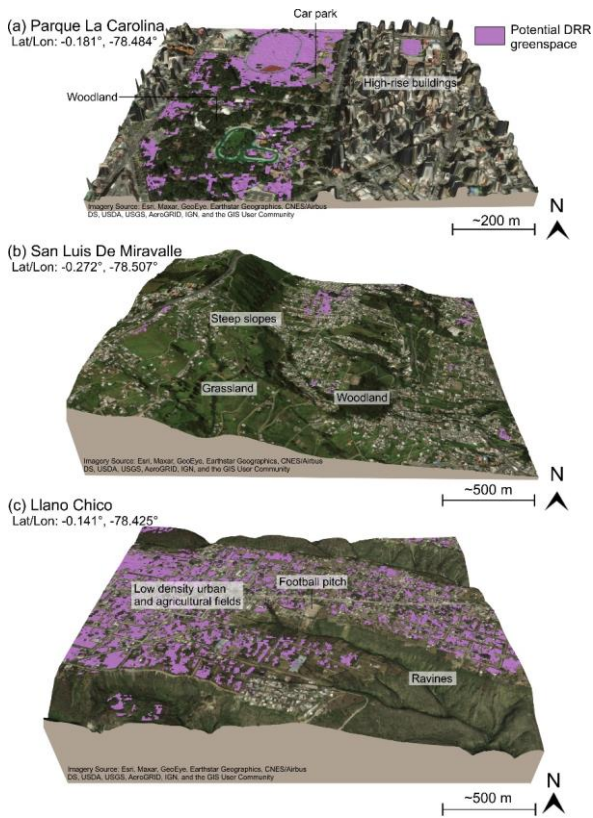
Deleted: ¶

570 communities can avoid damaged buildings and infrastructure and receive emergency aid (Sphere Association, 2018). These
571 spaces are increasingly viewed within a broader network of benefits to society and ecosystems (e.g. Fig.1a), and framed
572 within Eco-DRR strategies (UNDRR, 2020). We therefore evaluated greenspaces in Quito that could offer DRR capabilities
573 by both considering existing designated greenspaces and assessing other non-designated greenspaces.

574 **5.2 Greenspace**

575 Our study was designed to identify the basic requirements for sites that could be designated or developed as DRR greenspace
576 using an earth-observation based methodology that could be adapted and applied to other cities. This is timely since
577 greenspace is becoming increasingly desirable to improve environment quality, contribute to addressing climate breakdown,
578 and greenspace within Eco-DRR strategies can simultaneously mitigate against multiple hazards (Onuma and Tsuge, 2018;
579 McVittie et al., 2018; Sudmeier-Rieux et al., 2021). Our DRR greenspace primarily addresses the basic requirements of
580 people-space and amenable topography for medium- to long-term accommodation requirements, such as following a major
581 earthquake. Examples are shown in Fig. 12 for areas in central Quito and on the periphery. Regarding urban risk, green space
582 in Quito has been thought of from the perspective of threat. For example, interventions have been developed on the slopes of
583 Pichincha from a logic of risk mitigation (Vidal et al., 2015). Recently, after the 2016 Ecuador earthquake, green and open
584 spaces were incorporated throughout the city as safe points in case of evacuation (Rebotier, 2016) (Fig. 10a).
585

Deleted: Figure



587
 588 **Figure 12: 3D perspective showing examples of potential DRR greenspace identified in Quito. (a) Parque La Carolina is in central**
 589 **Quito amongst commercial high-rise buildings. (b) San Luis De Miravalle is located on the southeast of Quito and is characterised**
 590 **by lower density urban development and steep slopes. (c) Llano Chico is in the east of Quito with low density urban development**
 591 **mixed with agricultural land that is bounded by steep ravines.**

592 We found that 7% (2.5 km²) of the DMQ designated greenspace was identified as potential DRR greenspace. Similarly, 10%
 593 (1.7 km²) of the DMQ designated safe spaces intersected with our classified DRR greenspace (Fig. 8, 10a). The total area of
 594 potential DRR greenspace within Quito was 18.6 km², therefore large potential exists to incorporate new greenspaces into a
 595 DRR framework, especially in the south and east of the city, which are locations of projected future expansion and where
 596 urban expansion and population densities are lower (Fig. 5b, 9d). New designation of greenspaces could address some of the
 597 imbalance between greenspace access since 98% (~2.3 million) of Quito's population were within 800 m of a designated
 598 greenspace, compared to 2.1 million for the DRR greenspace (88%) (Fig. 9a). Lower socioeconomic classifications had a

599 greater distance to travel to the nearest designated greenspace, and a lower greenspace area per person overall (Fig. 9b, c),
600 which was also observed by Cuvi et al. (2021), noting that informal developments have less access to larger designated
601 parks. We found a median designated greenspace of 3 m² per person for the ‘low’ socioeconomic classification. However,
602 the availability of potential DRR greenspace to these same communities (median of 24 m²) shows that additional
603 designations could help address the imbalance. This is also aligned with Quito’s Vision 2040 document to increase
604 greenspace in urban areas to ~9 m² per person (DMQ, 2018). Critical to addressing these inequalities is to ensure that all
605 formal and informal settlements are reflected in socioeconomic statistics and included in official maps.

606
607 Although we found high accessibility of greenspace within 800 m of populations, the capacity to serve surrounding
608 populations for emergency refuge was 1.7% considering the recommended space allocation of 45 m² per person (Fig.
609 9a)(Sphere Association, 2018). Incorporating all additional spaces that are DRR suitable could increase this to 8%, or 40%
610 using a minimum living allocation of 3 m² per person (Sphere Association, 2018). A network analysis producing a ranked
611 top ten DRR greenspaces (Fig. 11) showed that eight intersected with currently designated greenspaces or safe spaces and
612 two did not. These two spaces could be investigated for negotiating formal access to these spaces for use in an emergency,
613 such as the golf course forming Site 5 (Fig. 11e).

614
615 We focus on greenspace as an emergency refuge; however, these spaces can also contribute to mitigating hazards both
616 through physical processes such as water retention or slope stabilisation (Phillips and Marden, 2005; Maragno et al., 2018;
617 Sandholz et al., 2018), and also by their existence in places that would be hazardous if urbanised. We found that of the
618 potential DRR greenspace identified in Quito, 62% intersected with TWI values indicative of potential flooding (section
619 4.2), 10% with areas of high landslide susceptibility, and 6% with both hazards (Fig. 8 – red circles). Therefore, there is
620 potential to mitigate future risk by maintaining greenspace and therefore avoiding development in potentially hazardous
621 areas, and incorporating additional DRR greenspaces that are not exposed to hazards for use as refuges.

622 5.3 Future work

623 Our study has provided a city-wide assessment of Quito’s historical and future growth projections, and the potential role of
624 greenspace in reducing disaster risk. The first-pass analysis of greenspace suitable for DRR could be used for local
625 community-scale evaluation and stakeholder engagement to deliver improved resilience for the city. Subsequently, the
626 methodology could be expanded to define a continuum of greenspace suitability for DRR by incorporating other important
627 factors including site specific suitability trade-offs such as land value, ownership, and access to water, electricity, and
628 hospitals (Anhorn and Khazai, 2015; Hosseini et al., 2016). Similarly, we focussed on greenspaces since these spaces are
629 most likely to be accessible and they provide multiple benefits; however, concreted grey spaces such as commercial car
630 parks could also serve a role in providing safe spaces for DRR, particularly if a disaster event occurred during work hours.
631 Methodological developments could include multi-temporal and potentially higher resolution datasets, for example landslide

Deleted:

Deleted: club

Deleted: improvements

635 susceptibility information that reflects changing land cover and therefore an evolving hazard (Emberson et al., 2020). For
636 example, a dynamic landslide susceptibility map could consider a potentially increased landslide hazard due to road cuttings
637 in areas undergoing urban development (Froude and Petley, 2018), and the dynamic nature of landslide hazard in response to
638 precipitation events (Kirschbaum and Stanley, 2018). Additionally, our investigation of flood events alongside a TWI would
639 benefit from a better understanding of the capacity and distribution of the subsurface drainage network within Quito,
640 particularly where natural drainage channels are blocked (e.g. Aragundi et al., 2016). Nonetheless, our assumptions that all
641 flood water would flow on the surface represents a worst-case scenario during a flood event where the artificial drainage
642 network is at capacity.

644 Use of EO-based datasets broadens the applicability of our methods to other cities. Whilst other sources of multi-spectral
645 satellite imagery (e.g. 3 m resolution PlanetScope or 10 m resolution Sentinel-2) could still delineate the types of greenspaces
646 relevant to DRR (e.g. Fig. 8 inset), we relied on a high resolution Pleiades DEM to provide topographic relief information on
647 the greenspace DRR suitability. Global 30 m resolution DEMs could likely substitute this in some cases, though they are
648 potentially less suitable in densely built urban environment where flat open greenspaces are interspaced with tall buildings
649 and trees for example (Fig. 12a), which cannot be distinguished in 30 m elevation models. Here, elevation and slope values
650 derived from 30 m resolution DEM represent an average of features (for example buildings, cars, and trees) within the 30 m
651 cell. Therefore, the topography of greenspaces is resolved in less detail.

Deleted: coarser resolution

Deleted: not

Deleted: resolved

652 6 Conclusion

653 In this study, we used a combination of satellite data analysis and secondary datasets to quantify Quito's historical growth,
654 future intersection with hazards, and distribution of greenspace within the city. Quito's historical growth (~192 km² 1986 to
655 2020) was primarily on flatter, former agricultural land, hence there was limited encroachment towards hazards of Pichincha
656 volcano and areas of higher landslide susceptibility. However, our work shows that future urbanisation projections suggest
657 an increasing intersection between urban areas and areas of high landslide susceptibility, which requires risk-informed
658 planning to mitigate. General accessibility of greenspaces is high, with 98% (2.3 million) of Quito's population within 800 m
659 of a designated greenspace and 88% (2.1 million) for the DRR greenspace classification. However, within 800 m, the
660 capacity of currently designated greenspaces and safe spaces would only fulfil 2% of Quito's population if required for
661 emergency refuge. Over 40% could be accommodated by incorporating new DRR greenspaces identified in this study. We
662 also found a disparity between access to greenspaces across socio-economic classifications, with low-medium groups having
663 less access to designated greenspace (3 m² per person for the 'low' classification compared to 8 m² for 'high'). In some
664 cases, these low-medium groups have the greatest opportunity for future designation of DRR greenspace due to their location
665 on the city periphery in areas of lower population density. Our workflow uses satellite data to provide a first-pass evaluation
666 of DRR greenspace potential and could therefore be adapted for application in other urbanising cities. The results provide the

Formatted: Font: 10 pt, Superscript

Formatted: Font: 10 pt

Formatted: Font: 10 pt, Superscript

Formatted: Font: 10 pt

Deleted: developing

671 foundation to evaluate these spaces with stakeholders at community to city-wide scales, since promoting equitable access to
672 greenspaces, communicating their multiple benefits, and considering their use to restrict development in hazardous areas will
673 be key to sustainable, risk-informed urban growth.

674 **Data availability**

675 The data used to support the findings and results of this study are available in the supplementary information and in the
676 Zenodo repository <https://doi.org/10.5281/zenodo.5881876>. Pleiades imagery data were provided through the CEOS Seismic
677 Hazard Demonstrator and are restricted by license.

678 **Author contribution**

679 All authors have read and agreed to the published version of the manuscript. CSW, ES, MAV, JRE, and SKE designed the
680 concept. JRE, CZ, SB-B, PC, DFO provided access to datasets. CSW performed the analysis and prepared the figures. CSW
681 wrote the manuscript with input from all authors.

682 **Competing interests**

683 The authors declare that they have no conflict of interest.

684 **Financial support**

685 This research has been supported the UK Research and Innovation (UKRI) Global Challenges Research Fund (GCRF) Urban
686 Disaster Risk Hub (NE/S009000/1) (Tomorrow's Cities), a NERC Innovation award (grant number NE/S013911/1), and
687 COMET. COMET is the NERC Centre for the Observation and Modelling of Earthquakes, Volcanoes and Tectonics, a
688 partnership between UK Universities and the British Geological Survey. John Elliott is supported by a Royal Society
689 University Research fellowship (UF150282), and Susanna Ebmeier is supported by a NERC Independent Research
690 Fellowship (NE/R015546/1).

691 **Acknowledgments**

692 The Committee on Earth Observation Satellites (CEOS) and Centre National d'Etudes Spatiales (CNES) are thanked for
693 providing access to the Pleiades satellite imagery used in this study. Pleiades images were made available by CNES in the
694 framework of the CEOS Working Group for Disasters. © CNES (2018, 2019, 2020), and Airbus DS, all rights reserved.
695 Commercial uses forbidden.

Deleted: .

Deleted: .

698 **References**

- 699 Airbus Defence and Space: Pléiades Imagery User Guide. [Accessed 29th October 2019] Available from:
700 <https://www.intelligence-airbusds.com/en/8718-user-guides>, 2012.
- 701 Allan, P., Bryant, M., Wirsching, C., Garcia, D., and Teresa Rodriguez, M.: The Influence of Urban Morphology on the
702 Resilience of Cities Following an Earthquake, *Journal of Urban Design*, 18, 242-262, 10.1080/13574809.2013.772881, 2013.
- 703 Altieri, M. A., Companioni, N., Cañizares, K., Murphy, C., Rosset, P., Bourque, M., and Nicholls, C. I.: The greening of the
704 “barrios”: Urban agriculture for food security in Cuba, *Agriculture and Human Values*, 16, 131-140,
705 10.1023/A:1007545304561, 1999.
- 706 Alvarado, A., Audin, L., Nocquet, J. M., Lagreulet, S., Segovia, M., Font, Y., Lamarque, G., Yepes, H., Mothes, P.,
707 Rolandone, F., Jarrín, P., and Quidelleur, X.: Active tectonics in Quito, Ecuador, assessed by geomorphological studies, GPS
708 data, and crustal seismicity, 33, 67-83, 10.1002/2012tc003224, 2014.
- 709 Amey, R. M. J., Elliott, J. R., Hussain, E., Walker, R., Pagani, M., Silva, V., Abdrakhmatov, K. E., and Watson, C. S.:
710 Significant Seismic Risk Potential from Buried Faults Beneath Almaty City, Kazakhstan, revealed from high-resolution
711 satellite DEMs, *Earth and Space Science*, <https://doi.org/10.1029/2021EA001664>, 2021.
- 712 Anhorn, J., and Khazai, B.: Open space suitability analysis for emergency shelter after an earthquake, *Nat. Hazards Earth*
713 *Syst. Sci.*, 15, 789-803, 10.5194/nhess-15-789-2015, 2015.
- 714 Aragundi, S. M., Mena, A. P., and Zamora, J. J.: Historical Urban Landscape as a Descriptive Feature for Risk Assessment:
715 the “Quebradas” of Quito, FICUP. An International Conference on Urban Physics, Quito – Galápagos, Ecuador, 2016.
- 716 Aronson, M. F., Lepczyk, C. A., Evans, K. L., Goddard, M. A., Lerman, S. B., MacIvor, J. S., Nilon, C. H., and Vargo, T.:
717 Biodiversity in the city: key challenges for urban green space management, *Frontiers in Ecology and the Environment*, 15,
718 189-196, <https://doi.org/10.1002/fee.1480>, 2017.
- 719 Baker, J. L.: Climate Change, Disaster Risk, and the Urban Poor, *Climate Change, Disaster Risk, and the Urban Poor*, 2012.
- 720 Bauwelinck, M., Casas, L., Nawrot, T. S., Nemery, B., Trabelsi, S., Thomas, I., Aerts, R., Lefebvre, W., Vanpoucke, C., Van
721 Nieuwenhuysse, A., Deboosere, P., and Vandenneede, H.: Residing in urban areas with higher green space is associated with
722 lower mortality risk: A census-based cohort study with ten years of follow-up, *Environment International*, 148, 106365,
723 <https://doi.org/10.1016/j.envint.2020.106365>, 2021.
- 724 Beauval, C., Marinier, J., Yepes, H., Audin, L., Nocquet, J. M., Alvarado, A., Baize, S., Aguilar, J., Singaicho, J., and
725 Jomard, H.: A New Seismic Hazard Model for Ecuador, *Bulletin of the Seismological Society of America*, 108,
726 10.1785/0120170259, 2018.
- 727 Benedict, M., and MacMahon, E.: *Green Infrastructure: Smart Conservation for the 21st Century*, 2002.
- 728 Beven, K. J., and Kirkby, M. J.: A physically based, variable contributing area model of basin hydrology / Un modèle à base
729 physique de zone d'appel variable de l'hydrologie du bassin versant, *Hydrological Sciences Bulletin*, 24, 43-69,
730 10.1080/02626667909491834, 1979.
- 731 Bonilla-Bedoya, S., Estrella, A., Vaca Yáñez, A., and Herrera, M. Á.: Urban socio-ecological dynamics: applying the urban-
732 rural gradient approach in a high Andean city, *Landscape Research*, 45, 327-345, 10.1080/01426397.2019.1641589, 2020a.

- 733 Bonilla-Bedoya, S., Mora, A., Vaca, A., Estrella, A., and Herrera, M. Á.: Modelling the relationship between urban
 734 expansion processes and urban forest characteristics: An application to the Metropolitan District of Quito, *Computers,
 735 Environment and Urban Systems*, 79, 101420, <https://doi.org/10.1016/j.compenvurbsys.2019.101420>, 2020b.
- 736 Borland, J.: Small parks, big designs: reconstructed Tokyo's new green spaces, 1923–1931, *Urban History*, 47, 106-125,
 737 10.1017/S0963926819000567, 2020.
- 738 Boulton, C., Dedekorkut-Howes, A., and Byrne, J.: Factors shaping urban greenspace provision: A systematic review of the
 739 literature, *Landscape and Urban Planning*, 178, 82-101, <https://doi.org/10.1016/j.landurbplan.2018.05.029>, 2018.
- 740 Bryant, M., and Allan, P.: Open space innovation in earthquake affected cities, in: *Approaches to Disaster Management -
 741 Examining the Implications of Hazards, Emergencies and Disasters*, edited by: (ed.), J. P. T., In-Tech, 2013.
- 742 Cardona, O., Aalst, M., Birkmann, J., Fordham, M., McGregor, G., Perez, R., Pulwarty, R., Schipper, L., and Sinh, B.:
 743 Determinants of risk: Exposure and vulnerability, in managing the risks of extreme events and disasters to advance climate
 744 change adaptation, 65-108 pp., 2012.
- 745 Carmin, J., and Anguelovski, I.: *Planning Climate Resilient Cities: Early Lessons from Early Adapters*, 2009.
- 746 Carrión, F., and Erazo Espinosa, J.: La forma urbana de Quito: una historia de centros y periferias, *Bulletin de l'Institut
 747 français d'études andines*, 503-522, 2012.
- 748 Castelo, C. A. J., D'Howitt, M. C., Almeida, O. P., and Toulkeridis, T.: Comparative Determination of the Probability of
 749 Landslide Occurrences and Susceptibility in Central Quito, Ecuador, 2018 International Conference on eDemocracy &
 750 eGovernment (ICEDEG), 2018, 136-143,
- 751 Chatelain, J. L., Tucker, B., Guillier, B., Kaneko, F., Yepes, H., Fernandez, J., Valverde, J., Hoefer, G., Souris, M., Dupérier,
 752 E., Yamada, T., Bustamante, G., and Villacis, C.: Earthquake risk management pilot project in Quito, Ecuador, *GeoJournal*,
 753 49, 185-196, 10.1023/A:1007079403225, 1999.
- 754 Colding, J., and Barthel, S.: The potential of 'Urban Green Commons' in the resilience building of cities, *Ecological
 755 Economics*, 86, 156-166, <https://doi.org/10.1016/j.ecolecon.2012.10.016>, 2013.
- 756 Cuví, N., and Vélez, L. C. G.: Los Parques Urbanos de Quito: Distribución, Accesibilidad y Segregación Espacial,
 757 *Environmental Science*, 10, 2021.
- 758 De Sherbinin, A., Schiller, A., and Pulsipher, A.: The vulnerability of global cities to climate hazards, *Environment and
 759 Urbanization*, 19, 39-64, 10.1177/0956247807076725, 2007.
- 760 Deng, J., Huang, Y., Chen, B., Tong, C., Liu, P., Wang, H., and Hong, Y.: A Methodology to Monitor Urban Expansion and
 761 Green Space Change Using a Time Series of Multi-Sensor SPOT and Sentinel-2A Images, *Remote Sensing*, 11, 1230, 2019.
- 762 DMQ: *Visión de Quito 2040 y su Nuevo Modelo de Ciudad*, 2018.
- 763 Domínguez-Castro, F., García-Herrera, R., and Vicente-Serrano, S. M.: Wet and dry extremes in Quito (Ecuador) since the
 764 17th century, *International Journal of Climatology*, 38, 2006-2014, 10.1002/joc.5312, 2018.
- 765 Dou, K., and Zhan, Q.: Accessibility analysis of urban emergency shelters: Comparing gravity model and space syntax, 2011
 766 International Conference on Remote Sensing, Environment and Transportation Engineering, 2011, 5681-5684,

767 Emberson, R., Kirschbaum, D., and Stanley, T.: New global characterisation of landslide exposure, *Nat. Hazards Earth Syst.*
768 *Sci.*, 20, 3413-3424, 10.5194/nhess-20-3413-2020, 2020.

769 Escobedo, F. J., and Nowak, D. J.: Spatial heterogeneity and air pollution removal by an urban forest, *Landscape and Urban*
770 *Planning*, 90, 102-110, <https://doi.org/10.1016/j.landurbplan.2008.10.021>, 2009.

771 Estrella, M., and Saalimaa, N.: Ecosystem-based disaster risk reduction (Eco-DRR): An overview, *The role of ecosystems*
772 *in disaster risk reduction*, edited by: Renaud, F. G., Sudmeier-Rieux, K., and Estrella, M., United Nations University Press,
773 2013.

774 Faivre, N., Sgobbi, A., Happaerts, S., Raynal, J., and Schmidt, L.: Translating the Sendai Framework into action: The EU
775 approach to ecosystem-based disaster risk reduction, *International Journal of Disaster Risk Reduction*, 32, 4-10,
776 <https://doi.org/10.1016/j.ijdrr.2017.12.015>, 2018.

777 Farr, T. G., Rosen, P. A., Caro, E., Crippen, R., Duren, R., Hensley, S., Kobrick, M., Paller, M., Rodriguez, E., Roth, L.,
778 Seal, D., Shaffer, S., Shimada, J., Umland, J., Werner, M., Oskin, M., Burbank, D., and Alsdorf, D.: The Shuttle Radar
779 Topography Mission, *Reviews of Geophysics*, 45, 10.1029/2005RG000183, 2007.

780 Fenger, J.: Urban air quality, *Atmospheric Environment*, 33, 4877-4900, [https://doi.org/10.1016/S1352-2310\(99\)00290-3](https://doi.org/10.1016/S1352-2310(99)00290-3),
781 1999.

782 Flörke, M., Schneider, C., and McDonald, R. I.: Water competition between cities and agriculture driven by climate change
783 and urban growth, *Nature Sustainability*, 1, 51-58, 10.1038/s41893-017-0006-8, 2018.

784 Froude, M. J., and Petley, D. N.: Global fatal landslide occurrence from 2004 to 2016, *Nat. Hazards Earth Syst. Sci.*, 18,
785 2161-2181, 10.5194/nhess-18-2161-2018, 2018.

786 Fuller, R., Groom, G., and Jones, A.: The land-cover map of great Britain: an automated classification of landsat thematic
787 mapper data, *Photogrammetric Engineering and Remote Sensing*, 60, 553-562, 1994.

788 Galasso, C., McCloskey, J., Pelling, M., Hope, M., Bean, C. J., Cremen, G., Guragain, R., Hancilar, U., Menoscal, J.,
789 Mwang'a, K., Phillips, J., Rush, D., and Sinclair, H.: Editorial. Risk-based, Pro-poor Urban Design and Planning for
790 Tomorrow's Cities, *International Journal of Disaster Risk Reduction*, 58, 102158,
791 <https://doi.org/10.1016/j.ijdrr.2021.102158>, 2021.

792 García-Lamarca, M., Connolly, J., and Anguelovski, I.: Green gentrification and displacement in Barcelona, in: *Housing*
793 *Displacement*, Routledge, 156-170, 2020.

794 Georganos, S., Grippa, T., Vanhuysse, S., Lennert, M., Shimoni, M., and Wolff, E.: Very High Resolution Object-Based
795 Land Use–Land Cover Urban Classification Using Extreme Gradient Boosting, *IEEE Geoscience and Remote Sensing*
796 *Letters*, 15, 607-611, 10.1109/LGRS.2018.2803259, 2018.

797 Gill, J. C., and Malamud, B. D.: Anthropogenic processes, natural hazards, and interactions in a multi-hazard framework,
798 *Earth-Science Reviews*, 166, 246-269, <https://doi.org/10.1016/j.earscirev.2017.01.002>, 2017.

799 Gill, J. C., Hussain, E., and Malamud, B. D.: Workshop Report: Multi-Hazard Risk Scenarios for Tomorrow's Cities.
800 [Accessed 18th May 2021]. Available from: [https://tomorrowscities.org/workshop-report-multi-hazard-risk-scenarios-](https://tomorrowscities.org/workshop-report-multi-hazard-risk-scenarios-tomorrows-cities)
801 [tomorrows-cities](https://tomorrowscities.org/workshop-report-multi-hazard-risk-scenarios-tomorrows-cities), 2021.

- 802 Godfray, H. C. J., Beddington, J. R., Crute, I. R., Haddad, L., Lawrence, D., Muir, J. F., Pretty, J., Robinson, S., Thomas, S.
803 M., and Toulmin, C.: Food Security: The Challenge of Feeding 9 Billion People, *Science*, 327, 812-818,
804 10.1126/science.1185383, 2010.
- 805 Gonzalez, C. G.: Seasons of Resistance: Sustainable Agriculture and Food Security in Cuba, *Tulane Environmental Law*
806 *Journal*, 16, 685-732, 2003.
- 807 Gorelick, N., Hancher, M., Dixon, M., Ilyushchenko, S., Thau, D., and Moore, R.: Google Earth Engine: Planetary-scale
808 geospatial analysis for everyone, *Remote Sensing of Environment*, 202, 18-27, <https://doi.org/10.1016/j.rse.2017.06.031>,
809 2017.
- 810 Gregory McPherson, E.: Accounting for benefits and costs of urban greenspace, *Landscape and Urban Planning*, 22, 41-51,
811 [https://doi.org/10.1016/0169-2046\(92\)90006-L](https://doi.org/10.1016/0169-2046(92)90006-L), 1992.
- 812 Hall, M. L., Samaniego, P., Le Pennec, J. L., and Johnson, J. B.: Ecuadorian Andes volcanism: A review of Late Pliocene to
813 present activity, *Journal of Volcanology and Geothermal Research*, 176, 1-6,
814 <https://doi.org/10.1016/j.jvolgeores.2008.06.012>, 2008.
- 815 Hastenrath, S.: Annual cycle of upper air circulation and convective activity over the tropical Americas, *Journal of*
816 *Geophysical Research: Atmospheres*, 102, 4267-4274, <https://doi.org/10.1029/96JD03122>, 1997.
- 817 Hoekstra, A. Y., Buurman, J., and van Ginkel, K. C. H.: Urban water security: A review, *Environ. Res. Lett.*, 13, 053002,
818 10.1088/1748-9326/aaba52, 2018.
- 819 Hosseini, S. A., de la Fuente, A., and Pons, O.: Multicriteria decision-making method for sustainable site location of post-
820 disaster temporary housing in urban areas, *Journal of Construction Engineering and Management*, 142, 04016036, 2016.
- 821 IG-EPN, IGM, IRD.: Mapa de Peligros Volcánicos Potenciales del Volcán Guagua Pichincha 3ra. Edición, Quito - Ecuador.
822 Available online: <https://www.igepn.edu.ec/ggp-mapa-de-peligros/file> (accessed 10 December 2020). 2019.
- 823 Inglada, J., and Christophe, E.: The Orfeo Toolbox remote sensing image processing software, 2009 IEEE International
824 Geoscience and Remote Sensing Symposium, 2009, IV-733-IV-736,
- 825 Instituto Geográfico Militar: Fotografía aérea 360 Rollo 19 Cámara RC10 Proyecto Carta Nacional N-III_1977 Escala
826 1:60000 B/N. [online]. Accessed: 20 March 2020. Available from:
827 <http://www.geoportalmgm.gob.ec/geonetwork/srv/spa/catalog.search#/metadata/e56534b0-3b16-423e-a076-e0e41df07a81>,
828 1977.
- 829 Instituto Geográfico Militar: Generation of geospatial information at a scale 1: 5 000 for the determination of the physical
830 fitness of the territory and urban development through the use of geotechnologies [Spanish], 2019.
- 831 Jalayer, F., De Risi, R., De Paola, F., Giugni, M., Manfredi, G., Gasparini, P., Topa, M. E., Yonas, N., Yeshitela, K.,
832 Nebebe, A., Cavan, G., Lindley, S., Printz, A., and Renner, F.: Probabilistic GIS-based method for delineation of urban
833 flooding risk hotspots, *Natural Hazards*, 73, 975-1001, 10.1007/s11069-014-1119-2, 2014.
- 834 James, P., Banay, R. F., Hart, J. E., and Laden, F.: A Review of the Health Benefits of Greenness, *Current Epidemiology*
835 *Reports*, 2, 131-142, 10.1007/s40471-015-0043-7, 2015.

- 836 Jeong, D., Kim, M., Song, K., and Lee, J.: Planning a Green Infrastructure Network to Integrate Potential Evacuation Routes
837 and the Urban Green Space in a Coastal City: The Case Study of Haeundae District, Busan, South Korea, *Science of The*
838 *Total Environment*, 761, 143179, <https://doi.org/10.1016/j.scitotenv.2020.143179>, 2021.
- 839 Kelleher, C., and McPhillips, L.: Exploring the application of topographic indices in urban areas as indicators of pluvial
840 flooding locations, *Hydrological Processes*, 34, 780-794, 2020.
- 841 Kennedy, R. E., Yang, Z., Gorelick, N., Braaten, J., Cavalcante, L., Cohen, W. B., and Healey, S.: Implementation of the
842 LandTrendr Algorithm on Google Earth Engine, *Remote Sensing*, 10, 691, 2018.
- 843 Khazai, B., Anhorn, J., Girard, T., Brink, S., Daniell, J., Bessel, T., Mühr, B., Flörchinger, V., and Kunz-Plapp, T.: Shelter
844 response and vulnerability of displaced populations in the April 25, 2015 Nepal Earthquake, Center for Disaster
845 Management and Risk Reduction Technology of the Karlsruhe Institute of Technology, and the South Asia Institute,
846 Heidelberg University, 5, 2015, 2015.
- 847 Kılıç, F., Kara, B. Y., and Bozkaya, B.: Locating temporary shelter areas after an earthquake: A case for Turkey, *European*
848 *Journal of Operational Research*, 243, 323-332, <https://doi.org/10.1016/j.ejor.2014.11.035>, 2015.
- 849 Kirschbaum, D., Stanley, T., and Yatheendradas, S.: Modeling landslide susceptibility over large regions with fuzzy overlay,
850 *Landslides*, 13, 485-496, 10.1007/s10346-015-0577-2, 2016.
- 851 Kirschbaum, D., and Stanley, T.: Satellite-Based Assessment of Rainfall-Triggered Landslide Hazard for Situational
852 Awareness, *Earth's Future*, 6, <https://doi.org/doi:10.1002/2017EF000715>, 2018.
- 853 Kumar, P., Debele, S. E., Sahani, J., Rawat, N., Marti-Cardona, B., Alfieri, S. M., Basu, B., Basu, A. S., Bowyer, P.,
854 Charizopoulos, N., Jaakko, J., Loupis, M., Menenti, M., Mickovski, S. B., Pfeiffer, J., Pilla, F., Pröll, J., Pulvirenti, B.,
855 Rutzinger, M., Sannigrahi, S., Spyrou, C., Tuomenvirta, H., Vojinovic, Z., and Zieher, T.: An overview of monitoring
856 methods for assessing the performance of nature-based solutions against natural hazards, *Earth-Science Reviews*, 217,
857 103603, <https://doi.org/10.1016/j.earscirev.2021.103603>, 2021.
- 858 Labib, S. M., and Harris, A.: The potentials of Sentinel-2 and LandSat-8 data in green infrastructure extraction, using object
859 based image analysis (OBIA) method, *European Journal of Remote Sensing*, 51, 231-240, 10.1080/22797254.2017.1419441,
860 2018.
- 861 Leblon, B., Gallant, L., and Granberg, H.: Effects of shadowing types on ground-measured visible and near-infrared shadow
862 reflectances, *Remote Sensing of Environment*, 58, 322-328, [https://doi.org/10.1016/S0034-4257\(96\)00079-X](https://doi.org/10.1016/S0034-4257(96)00079-X), 1996.
- 863 Lidberg, W., Nilsson, M., Lundmark, T., and Ågren, A. M.: Evaluating preprocessing methods of digital elevation models
864 for hydrological modelling, *Hydrological Processes*, 31, 4660-4668, 2017.
- 865 Liu, Q., Ruan, X., and Shi, P.: Selection of emergency shelter sites for seismic disasters in mountainous regions: Lessons
866 from the 2008 Wenchuan Ms 8.0 Earthquake, China, *Journal of Asian Earth Sciences*, 40, 926-934, 2011.
- 867 Loughlin, S. C., Sparks, R. S. J., Sparks, S., Brown, S. K., Jenkins, S. F., and Vye-Brown, C.: *Global volcanic hazards and*
868 *risk*, Cambridge University Press, 2015.
- 869 Manfreda, S., Di Leo, M., and Sole, A.: Detection of flood-prone areas using digital elevation models, *Journal of Hydrologic*
870 *Engineering*, 16, 781-790, 2011.

871 Maragno, D., Gaglio, M., Robbi, M., Appiotti, F., Fano, E. A., and Gissi, E.: Fine-scale analysis of urban flooding reduction
872 from green infrastructure: An ecosystem services approach for the management of water flows, *Ecological Modelling*, 386,
873 1-10, <https://doi.org/10.1016/j.ecolmodel.2018.08.002>, 2018.

874 Markus, T., Neumann, T., Martino, A., Abdalati, W., Brunt, K., Csatho, B., Farrell, S., Fricker, H., Gardner, A., Harding, D.,
875 Jasinski, M., Kwok, R., Magruder, L., Lubin, D., Luthcke, S., Morison, J., Nelson, R., Neuenschwander, A., Palm, S.,
876 Popescu, S., Shum, C. K., Schutz, B. E., Smith, B., Yang, Y., and Zwally, J.: The Ice, Cloud, and land Elevation Satellite-2
877 (ICESat-2): Science requirements, concept, and implementation, *Remote Sensing of Environment*, 190, 260-273,
878 <https://doi.org/10.1016/j.rse.2016.12.029>, 2017.

879 Marmot, M., Friel, S., Bell, R., Houweling, T. A. J., and Taylor, S.: Closing the gap in a generation: health equity through
880 action on the social determinants of health, *The Lancet*, 372, 1661-1669, [https://doi.org/10.1016/S0140-6736\(08\)61690-6](https://doi.org/10.1016/S0140-6736(08)61690-6),
881 2008.

882 Marselle, M. R., Bowler, D. E., Watzema, J., Eichenberg, D., Kirsten, T., and Bonn, A.: Urban street tree biodiversity and
883 antidepressant prescriptions, *Scientific Reports*, 10, 22445, 10.1038/s41598-020-79924-5, 2020.

884 Mattivi, P., Franci, F., Lambertini, A., and Bitelli, G.: TWI computation: a comparison of different open source GISs, *Open*
885 *Geospatial Data, Software and Standards*, 4, 1-12, 2019.

886 McDonald, R. I., Mansur, A. V., Ascensão, F., Colbert, M. I., Crossman, K., Elmqvist, T., Gonzalez, A., Güneralp, B.,
887 Haase, D., Hamann, M., Hillel, O., Huang, K., Kahnt, B., Maddox, D., Pacheco, A., Pereira, H. M., Seto, K. C., Simkin, R.,
888 Walsh, B., Werner, A. S., and Ziter, C.: Research gaps in knowledge of the impact of urban growth on biodiversity, *Nature*
889 *Sustainability*, 3, 16-24, 10.1038/s41893-019-0436-6, 2020.

890 McVittie, A., Cole, L., Wreford, A., Sgobbi, A., and Yordi, B.: Ecosystem-based solutions for disaster risk reduction:
891 Lessons from European applications of ecosystem-based adaptation measures, *International Journal of Disaster Risk*
892 *Reduction*, 32, 42-54, <https://doi.org/10.1016/j.ijdr.2017.12.014>, 2018.

893 Metro Ecuador: En caso de un sismo en Quito, estos son los sitios seguros en la ciudad. Metro Ecuador. [Online]. 12
894 December. [Accessed 01 November 2021]. Available from: [https://www.metroecuador.com.ec/ec/noticias/2019/05/28/caso-](https://www.metroecuador.com.ec/ec/noticias/2019/05/28/caso-temblor-estos-los-sitios-seguros-quito.html)
895 [temblor-estos-los-sitios-seguros-quito.html](https://www.metroecuador.com.ec/ec/noticias/2019/05/28/caso-temblor-estos-los-sitios-seguros-quito.html), 2019.

896 Millard, K., and Richardson, M.: On the Importance of Training Data Sample Selection in Random Forest Image
897 Classification: A Case Study in Peatland Ecosystem Mapping, *Remote. Sens.*, 7, 8489-8515, 2015.

898 Ministry of Territory. Habitat and Housing.: Accidentes.
899 <https://territorio.maps.arcgis.com/home/item.html?id=5270bc85cf3249b29937d25d0b363396>, 2020.

900 Myint, S. W., Gober, P., Brazel, A., Grossman-Clarke, S., and Weng, Q.: Per-pixel vs. object-based classification of urban
901 land cover extraction using high spatial resolution imagery, *Remote Sensing of Environment*, 115, 1145-1161,
902 <http://dx.doi.org/10.1016/j.rse.2010.12.017>, 2011.

903 Neumann, T. A., Martino, A. J., Markus, T., Bae, S., Bock, M. R., Brenner, A. C., Brunt, K. M., Cavanaugh, J., Fernandes,
904 S. T., Hancock, D. W., Harbeck, K., Lee, J., Kurtz, N. T., Luers, P. J., Luthcke, S. B., Magruder, L., Pennington, T. A.,
905 Ramos-Izquierdo, L., Rebold, T., Skoog, J., and Thomas, T. C.: The Ice, Cloud, and Land Elevation Satellite – 2 mission: A
906 global geolocated photon product derived from the Advanced Topographic Laser Altimeter System, *Remote Sensing of*
907 *Environment*, 233, 111325, <https://doi.org/10.1016/j.rse.2019.111325>, 2019.

908 Neumann, T. A., Brenner, A., Hancock, D., Robbins, J., Saba, J., Harbeck, K., Gibbons, A., Lee, J., Luthcke, S. B., and
909 Rebold, T.: ATLAS/ICESat-2 L2A Global Geolocated Photon Data, Version 3. Boulder, Colorado USA. NASA National
910 Snow and Ice Data Center Distributed Active Archive Center. doi: <https://doi.org/10.5067/ATLAS/ATL03.003>. [Accessed
911 7th December 2020]. 2020.

912 Nuth, C., and Kääb, A.: Co-registration and bias corrections of satellite elevation data sets for quantifying glacier thickness
913 change, *The Cryosphere*, 5, 271-290, <https://doi.org/10.1016/10.5194/tc-5-271-2011>, 2011.

914 Oliver-Smith, A., Alcántara-Ayala, I., I, B., and Lavell, A.: Forensic Investigations of Disasters (FORIN): a conceptual
915 framework and guide to research. Available online: [http://www.irdrinternational.org/wp-content/uploads/2016/01/FORIN-2-
916 29022016.pdf](http://www.irdrinternational.org/wp-content/uploads/2016/01/FORIN-2-29022016.pdf)
917 (accessed on 11 November 2019). 2016.

918 Olofsson, P., Foody, G. M., Stehman, S. V., and Woodcock, C. E.: Making better use of accuracy data in land change
919 studies: Estimating accuracy and area and quantifying uncertainty using stratified estimation, *Remote Sensing of
920 Environment*, 129, 122-131, <https://doi.org/10.1016/j.rse.2012.10.031>, 2013.

921 Olofsson, P., Foody, G. M., Herold, M., Stehman, S. V., Woodcock, C. E., and Wulder, M. A.: Good practices for estimating
922 area and assessing accuracy of land change, *Remote Sensing of Environment*, 148, 42-57,
923 <https://doi.org/10.1016/j.rse.2014.02.015>, 2014.

924 Onuma, A., and Tsuge, T.: Comparing green infrastructure as ecosystem-based disaster risk reduction with gray
925 infrastructure in terms of costs and benefits under uncertainty: A theoretical approach, *International Journal of Disaster Risk
926 Reduction*, 32, 22-28, <https://doi.org/10.1016/j.ijdrr.2018.01.025>, 2018.

927 Pagani, M., Garcia-Pelaez, J., Gee, R., Johnson, K., Poggi, V., Styron, R., Weatherill, G., Simionato, M., Viganò, D.,
928 Danciu, L., and Monelli, D.: Global Earthquake Model (GEM) Seismic Hazard Map (version 2018.1 - December 2018).
929 Available online: <https://www.globalquakemodel.org/gem-maps/global-earthquake-hazard-map> (accessed 5 May 2021).
930 DOI: 10.13117/GEM-GLOBAL-SEISMIC-HAZARD-MAP-2018.1, 2018.

931 Passalacqua, P., Belmont, P., Staley, D. M., Simley, J. D., Arrowsmith, J. R., Bode, C. A., Crosby, C., DeLong, S. B., Glenn,
932 N. F., Kelly, S. A., Lague, D., Sangireddy, H., Schaffrath, K., Tarboton, D. G., Wasklewicz, T., and Wheaton, J. M.:
933 Analyzing high resolution topography for advancing the understanding of mass and energy transfer through landscapes: A
934 review, *Earth-Science Reviews*, 148, 174-193, <http://dx.doi.org/10.1016/j.earscirev.2015.05.012>, 2015.

935 Pelling, M., Maskrey, A., Ruiz, P., Hall, P., Peduzzi, P., Dao, Q.-H., Mouton, F., Herold, C., and Kluser, S.: Reducing
936 disaster risk: a challenge for development, 2004.

937 Peralta Arias, J. J., and Higuera García, E.: Evaluación sostenible de los Planes Directores de Quito. Periodo 1942-2012,
938 2016.

939 Perrin, J. L., Bouvier, C., Janeau, J. L., Ménez, G., and Cruz, F.: Rainfall/runoff processes in a small peri-urban catchment in
940 the Andes mountains. The Rumihurcu Quebrada, Quito (Ecuador), *Hydrological Processes*, 15, 843-854,
941 <https://doi.org/10.1002/hyp.190>, 2001.

942 Pettorelli, N., Vik, J. O., Mysterud, A., Gaillard, J.-M., Tucker, C. J., and Stenseth, N. C.: Using the satellite-derived NDVI
943 to assess ecological responses to environmental change, *Trends in Ecology & Evolution*, 20, 503-510,
944 <https://doi.org/10.1016/j.tree.2005.05.011>, 2005.

- 945 Phillips, C., and Marden, M.: Reforestation Schemes to Manage Regional Landslide Risk, in: *Landslide Hazard and Risk*,
946 517-547, 2005.
- 947 Rebotier, J.: *El riesgo y su gestión en Ecuador: una mirada de geografía social y política*, Centro de Publicaciones Pontificia
948 Universidad Católica del Ecuador, 2016.
- 949 Robin, C., Samaniego, P., Le Pennec, J.-L., Mothes, P., and van der Plicht, J.: Late Holocene phases of dome growth and
950 Plinian activity at Guagua Pichincha volcano (Ecuador), *Journal of Volcanology and Geothermal Research*, 176, 7-15,
951 <https://doi.org/10.1016/j.jvolgeores.2007.10.008>, 2008.
- 952 Rodriguez-Galiano, V. F., Ghimire, B., Rogan, J., Chica-Olmo, M., and Rigol-Sanchez, J. P.: An assessment of the
953 effectiveness of a random forest classifier for land-cover classification, *ISPRS Journal of Photogrammetry and Remote*
954 *Sensing*, 67, 93-104, <https://doi.org/10.1016/j.isprsjprs.2011.11.002>, 2012.
- 955 Salazar, E., Henríquez, C., Sliuzas, R., and Qüense, J.: Evaluating Spatial Scenarios for Sustainable Development in Quito,
956 Ecuador, *ISPRS Int. J. Geo Inf.*, 9, 141, 2020.
- 957 Salazar, E., Henríquez, C., Durán, G., Qüense, J., and Puente-Sotomayor, F.: How to Define a New Metropolitan Area? The
958 Case of Quito, Ecuador, and Contributions for Urban Planning, *Land*, 10, 413, 2021.
- 959 Salmon, N., Yépez, G., Duque, M., Yépez, M., Báez, A., Masache-Heredia, M., Mejía, G., Mejía, P., Garofalo, G., and
960 Montoya, D.: Co-design of a Nature-Based Solutions Ecosystem for Reactivating a Peri-Urban District in Quito, Ecuador, in:
961 *Governance of Climate Responsive Cities: Exploring Cross-Scale Dynamics*, edited by: Peker, E., and Ataöv, A., Springer
962 International Publishing, Cham, 79-104, 2021.
- 963 Sandholz, S., Lange, W., and Nehren, U.: Governing green change: Ecosystem-based measures for reducing landslide risk in
964 Rio de Janeiro, *International Journal of Disaster Risk Reduction*, 32, 75-86, <https://doi.org/10.1016/j.ijdrr.2018.01.020>, 2018.
- 965 Schneider, A., and Woodcock, C. E.: Compact, Dispersed, Fragmented, Extensive? A Comparison of Urban Growth in
966 Twenty-five Global Cities using Remotely Sensed Data, Pattern Metrics and Census Information, *Urban Studies*, 45, 659-
967 692, 10.1177/0042098007087340, 2008.
- 968 Shimpó, N., Wesener, A., and McWilliam, W.: How community gardens may contribute to community resilience following
969 an earthquake, *Urban Forestry & Urban Greening*, 38, 124-132, <https://doi.org/10.1016/j.ufug.2018.12.002>, 2019.
- 970 Shrestha, S. R., Sliuzas, R., and Kuffer, M.: Open spaces and risk perception in post-earthquake Kathmandu city, *Applied*
971 *Geography*, 93, 81-91, <https://doi.org/10.1016/j.apgeog.2018.02.016>, 2018.
- 972 Sierra, A.: *La política de mitigación de los riesgos en las laderas de Quito: ¿qué vulnerabilidad combatir?*, 2009,
- 973 SNI: *Archivos de Informacion Geografica. Peligro Volcánico* [Accessed 24 August 2020], 2020.
- 974 Sphere Association: *The Sphere Handbook: Humanitarian Charter and Minimum Standards in Humanitarian Response*,
975 fourth edition, Geneva, Switzerland,
976 www.spherestandards.org/handbook, 2018.
- 977 Stanley, T., and Kirschbaum, D. B.: A heuristic approach to global landslide susceptibility mapping, *Natural Hazards*, 87,
978 145-164, <https://doi.org/10.1007/s11069-017-2757-y>, 2017.

Field Code Changed

- 979 Styron, R.: GEMScienceTools/gem-global-active-faults: First release of 2019 (Version 2019.0), ZENODO,
980 <http://doi.org/10.5281/zenodo.3376300>, 2019.
- 981 Sudmeier-Rieux, K., Arce-Mojica, T., Boehmer, H. J., Doswald, N., Emerton, L., Friess, D. A., Galvin, S., Hagenlocher, M.,
982 James, H., Laban, P., Lacambra, C., Lange, W., McAdoo, B. G., Moos, C., Mysiak, J., Narvaez, L., Nehren, U., Peduzzi, P.,
983 Renaud, F. G., Sandholz, S., Schreyers, L., Sebesvari, Z., Tom, T., Triyanti, A., van Eijk, P., van Staveren, M., Vicarelli, M.,
984 and Walz, Y.: Scientific evidence for ecosystem-based disaster risk reduction, *Nature Sustainability*, 4, 803-810,
985 10.1038/s41893-021-00732-4, 2021.
- 986 Taylor, L., and Hochuli, D. F.: Defining greenspace: Multiple uses across multiple disciplines, *Landscape and Urban*
987 *Planning*, 158, 25-38, <https://doi.org/10.1016/j.landurbplan.2016.09.024>, 2017.
- 988 Testori, G.: *Gobierno Barrial de Atacucho. An urban alternative based on self-governance and direct democracy*, 2016.
- 989 Tidball, K. G., and Krasny, M. E.: *Greening in the red zone: Disaster, Resilience and Community Greening*, Springer, 2012.
- 990 Tucker, C. J., Holben, B. N., Elgin, J. H., and McMurtrey, J. E.: Remote sensing of total dry-matter accumulation in winter
991 wheat, *Remote Sensing of Environment*, 11, 171-189, [https://doi.org/10.1016/0034-4257\(81\)90018-3](https://doi.org/10.1016/0034-4257(81)90018-3), 1981.
- 992 UN-Habitat: *The Challenge of Slums: Global Report on Human Settlements 2003*. Availalbe online:
993 <https://www.alnap.org/help-library/the-challenge-of-slums-global-report-on-human-settlements-2003> (accessed on 4 May
994 2021), 2003.
- 995 UN DESA: *World Urbanization Prospects: The 2018 Revision (ST/ESA/SER.A/420)*. New York: United Nations., 2019.
- 996 UN General Assembly: *Transforming our world: the 2030 Agenda for Sustainable Development*. Report No. A/RES/70/1.,
997 2015.
- 998 Sendai framework for disaster risk reduction 2015 - 2030.:
999 https://www.preventionweb.net/files/43291_sendaiframeworkfordrren.pdf, access: 05 February 2020, 2015.
- 1000 UNDRR: *Ecosystem-Based Disaster Risk Reduction: Implementing Nature-based Solutions for Resilience*, United Nations
1001 Office for Disaster Risk Reduction – Regional Office for Asia and the Pacific, Bangkok, Thailand, 2020.
- 1002 Valcárcel, J., Despotaki, V., Burton, C., Yepes-Estrada, C., Silva, V., and Villacis, C.: *Integrated Assessment of Earthquake*
1003 *Risk in Quito, Ecuador Using Openquake*, 16th World Conference on Earthquake Engineering, 16WCEE 2017, 2017,
- 1004 Valencia, V. H., Levin, G., and Hansen, H. S.: *Modelling the spatial extent of urban growth using a cellular automata-based*
1005 *model: a case study for Quito, Ecuador*, *Geografisk Tidsskrift-Danish Journal of Geography*, 120, 156-173,
1006 10.1080/00167223.2020.1823867, 2020.
- 1007 Vidal, X., Burgos, L., and Zevallos, O.: *11 Protection and environmental restoration of the slopes of Pichincha in Quito,*
1008 *Ecuador, Water and Cities in Latin America: Challenges for Sustainable Development*, 181, 2015.
- 1009 Vincenti, S. S., Zuleta, D., Moscoso, V., Jácome, P., Palacios, E., and Villacís, M.: *Análisis estadístico de datos*
1010 *meteorológicos mensuales y diarios para la determinación de variabilidad climática y cambio climático en el Distrito*
1011 *Metropolitano de Quito, La Granja*, 16, 23-47, 2012.
- 1012 WHO Regional Office for Europe: *Urban green spaces and health.*, 2016.

1013 Wilson, T. M., Stewart, C., Sword-Daniels, V., Leonard, G. S., Johnston, D. M., Cole, J. W., Wardman, J., Wilson, G., and
1014 Barnard, S. T.: Volcanic ash impacts on critical infrastructure, *Physics and Chemistry of the Earth, Parts A/B/C*, 45-46, 5-23,
1015 <https://doi.org/10.1016/j.pce.2011.06.006>, 2012.

1016 Wolch, J. R., Byrne, J., and Newell, J. P.: Urban green space, public health, and environmental justice: The challenge of
1017 making cities 'just green enough', *Landscape and Urban Planning*, 125, 234-244,
1018 <https://doi.org/10.1016/j.landurbplan.2014.01.017>, 2014.

1019 Yamazaki, F., Liu, W., and Takasaki, M.: Characteristics of shadow and removal of its effects for remote sensing imagery,
1020 2009 IEEE International Geoscience and Remote Sensing Symposium, 4, <https://doi.org/10.1109/IGARSS.2009.5417404>,
1021 2009.

1022 Zalakeviciute, R., López-Villada, J., and Rybarczyk, Y.: Contrasted Effects of Relative Humidity and Precipitation on Urban
1023 PM2.5 Pollution in High Elevation Urban Areas, *Sustainability*, 10, 2064, 2018.

1024 Zambrano-Barragán, C., Zevallos, O., Villacís, M., and Enríquez, D.: Quito's Climate Change Strategy: A Response to
1025 Climate Change in the Metropolitan District of Quito, Ecuador, in: *Resilient Cities*, Dordrecht, 2011, 515-529,

1026 Zhou, Y., Parsons, B., Elliott, J. R., Barisin, I., and Walker, R. T.: Assessing the ability of Pleiades stereo imagery to
1027 determine height changes in earthquakes: A case study for the El Mayor-Cucapah epicentral area, *Journal of Geophysical*
1028 *Research: Solid Earth*, 120, 8793-8808, 10.1002/2015jb012358, 2015.

1029 Zhu, Z., Gallant, A. L., Woodcock, C. E., Pengra, B., Olofsson, P., Loveland, T. R., Jin, S., Dahal, D., Yang, L., and Auch,
1030 R. F.: Optimizing selection of training and auxiliary data for operational land cover classification for the LCMAP initiative,
1031 *ISPRS Journal of Photogrammetry and Remote Sensing*, 122, 206-221, <https://doi.org/10.1016/j.isprsjprs.2016.11.004>, 2016.
1032